How internal fins enhance the thermohydraulic performance of geothermal pipes: A direct numerical simulation study

International Journal of Heat and Mass Transfer 256 (2026) 128114

Contents lists available at ScienceDirect

International Journal of Heat and Mass Transfer

journal homepage: www.elsevier.com/locate/hmt

How internal fins enhance the thermohydraulic performance of geothermal pipes: A direct numerical simulation study

Niklas Hidman [a,*], Daniel Almgren [b], Kim Johansson [b], Eskil Nilsson [c]

[a] Department of Mechanics and Maritime Sciences, Chalmers University of Technology, Gothenburg, SE-412 96, Sweden
[b] MuoviTech Sweden AB, Brämhult, SE-507 30, Sweden
[c] Ernströmgruppen AB, Gothenburg, SE-411 10, Sweden

ARTICLE INFO

Keywords:
Geothermal collector
Internally finned pipe
Alternating helical fins
Heat transfer enhancement
Turbulence trigger
Low pressure drop
DNS

ABSTRACT

Geothermal heat exchanger systems provide stable, efficient, and sustainable heating and cooling solutions. Their performance can be enhanced by achieving more effective convective heat transfer in the collector pipes without causing excessive pressure drop. This study investigates the use of internal fins in pipes as a means to improve the thermohydraulic performance under operating conditions typical of geothermal applications (Reynolds numbers $1300 \leq Re \leq 3300$ and Prandtl numbers $20 \leq Pr \leq 75$). Direct numerical simulations are employed to examine three fin configurations: straight axial fins, continuous helical fins, and fins with alternating helical orientations along the pipe axis. The alternating helical fin design is shown to trigger an unsteady flow at significantly lower Re than the other designs. Using the alternating design, we analyse the influence of the fin height, number of fins and fin twist rate on the thermohydraulic performance. The results demonstrate that the proposed alternating helical configuration triggers unsteady flow down to $1700 < Re < 1800$ while maintaining nearly the same friction factor as a smooth pipe at both $Re \leq 1700$ and $Re \geq 2300$. The augmented flow gives 3–6 times higher heat transfer compared to a smooth pipe in the interval $1700 < Re < 2300$. The findings highlight a promising fin design strategy for geothermal systems where minimizing pressure losses is essential, and they facilitate general guidelines for developing efficient fin-enhanced heat exchanger pipes in related applications operating under similar conditions.

1. Introduction

Geothermal systems are increasingly used to meet the growing global demand for sustainable energy, mainly because they are available essentially everywhere and the heat is continuously replenished, facilitating non-intermittent base load production [1,2]. Near-surface, or shallow, geothermal systems (for example ground heat collectors and borehole heat exchangers) collect heat from the ground at depths of up to several hundred meters [3]. These geothermal systems deliver steady and reliable heat production with excellent energy efficiency, typically providing 2–5 times higher thermal energy than the electric energy consumed during the operation of the system [4].

The most common systems include a heat pump, a vertical (borehole) ground heat exchanger and a heat distribution system [4]. Here, we focus on vertical ground heat exchangers (VGHE), but the results are generally applicable also for horizontal heat exchangers. In these systems, the geothermal collector pipe is a key component, acting as the heat exchanger between the working fluid (often a water/antifreeze mixture referred to as the brine) and the surrounding ground. The collector pipe is most commonly a closed-loop U-tube made of high-density polyethylene that is inserted into the borehole [5].

Although VGHEs are efficient and reliable, the main drawback is the substantial investment involved in the drilling of the borehole [2]. The required depth and diameter of the borehole are often characterized by the borehole thermal resistance, which is the thermal resistance between the brine and the borehole wall [5,6]. Therefore, the drilling cost can potentially be reduced by reducing the borehole thermal resistance [5]. Reducing the borehole resistance can also make the heat pump system cheaper and more efficient [5]. One way of reducing the borehole thermal resistance is by reducing the convective thermal resistance of the brine in the collector pipe. In fact, lowering the resistance of the pipe can even reduce the effective thermal resistance of the grout in the borehole (this is because the latter resistance is based on the mean temperature at the outer pipe wall that is more uniform at lower pipe resistances), further enhancing the efficiency of the geothermal system [4]. Therefore, enhancing the thermohydraulic performance of the collector pipes can significantly improve the overall efficiency and

* Corresponding author.
E-mail address: niklas.hidman@chalmers.se (N. Hidman).

https://doi.org/10.1016/j.ijheatmasstransfer.2025.128114
Received 15 August 2025; Received in revised form 6 November 2025; Accepted 13 November 2025
Available online 24 November 2025

Nomenclature

Δ	Computational grid spacing [m]
Δp	Pressure difference [Pa]
ϵ	Energy dissipation rate per unit mass [m^2/s]
ε	Pipe effective roughness height [m]
η	Kolmogorov length scale [m]
μ	Dynamics viscosity [kg/(ms)]
ν	Kinematic viscosity [m^2/s]
Ω	Volume [m^3]
ω_{fin}	Fin twist rate [°]
$\omega_x = \partial u_z/\partial y - \partial u_y/\partial z$	Axial vorticity [s^{-1}]
ρ	Density [kg/m]
τ_w	Wall shear stress [Pa]
a_i	Non-dimensional uniform acceleration vector [−]
c_p	Specific heat capacity [J/(kg K)]
D	Pipe Diameter [m]
f	Darcy friction factor [−]
h	Convective heat transfer coefficient [$W/(m^2\ K)$]
h_{fin}	Fin height [m]
k	Thermal conductivity [W/(m K)]
L	Pipe length [m]
n_{fin}	Number of fins [−]
$Nu = hD/k$	Nusselt number [−]
P	Pump power [W]
p	Pressure [Pa]
$p^* = p/(\rho U_b^2)$	Non-dimensional pressure [−]
PEC	Performance Evaluation Criterion [−]
$Pr = c_p\mu/k$	Prandtl number [−]
q_w	Wall heat flux [W/m^2]
R	Pipe radius [m]
r	Pipe radial coordinate [m]
$Re = U_b D/\nu$	Reynolds number [−]
$Re_c = 2300$	Critical Reynolds number [−]
$\boldsymbol{S}$	Rate of deformation tensor [s^{-1}]
S_Q	Non-dimensional uniform cooling term [−]
T	Temperature [K]
t	Time [s]
$T^* = (T - T_b)/(T_w - T_b)$	Non-dimensional temperature [−]
$t^* = tU_b/D$	Non-dimensional time [−]
T_b	Bulk temperature [K]
T_w	Wall temperature [K]
u_i	Velocity vector [m/s]
$u_i^* = u_i/D$	Non-dimensional velocity vector [−]
U_b	Bulk velocity [m/s]
u_τ	Friction velocity [m/s]
x	Pipe axial (streamwise) coordinate [m]
$x_i^* = x_i/D$	Non-dimensional spatial coordinates [−]
y	Pipe vertical (cross-stream) coordinate [m]
$y^+ = yu_\tau/\nu$	Dimensionless wall distance [−]
z	Pipe horizontal (cross-stream) coordinate [m]

lower the investment costs of the geothermal system [2,4,7,8].

In traditional pipeline industries such as oil and gas transport, water distribution, and district heating, the modelling and analysis of pipeline systems remain highly challenging. System-scale predictions are complicated by the presence of geometric complexity (bends, junctions, and fittings), surface roughness/modifications, as well as unsteady operating conditions including start-up, shut-down, and transient demand [9]. In addition, multiphase effects (e.g., gas–liquid or particle-laden flows) and strong coupling between thermal and hydraulic phenomena further increase the difficulty of developing accurate and reliable models [10]. When thermal effects are involved, as in geothermal collector pipes, the situation becomes even more complex because heat transfer is strongly coupled with the hydrodynamics. To remain computationally affordable, industrial-scale models often rely on empirical correlations or reduced-order approaches, which may not provide sufficient accuracy across all operating regimes. High-fidelity simulations such as Direct Numerical Simulations (DNS), although limited to simplified geometries and moderate Reynolds numbers, provide valuable benchmark data and physical insight into the underlying thermohydraulic mechanisms. Such insights can facilitate the development of improved models and design strategies for applications where efficient heat transfer in pipe systems is critical, including borehole heat exchangers.

Heat transfer enhancement methods for heat exchanger pipes have been extensively studied before (in a wide range of heat exchanger applications) and can generally be classified into active or passive methods [11–13]. Active methods require an external power input and typically involve a more complicated design [14]. This makes active methods less suitable for collector pipes that should operate underground, without maintenance, for more than 50 years. On the other hand, passive methods generally involve surface or geometrical modifications of the heat exchanger pipe [15]. Such modifications are relatively straightforward to incorporate into conventional collector pipe production processes. For these reasons, we focus on passive methods in this work.

Most passive heat transfer enhancement techniques are either based on pipe inserts (such as twisted tape [16,17], wire coils [18] or finned structures [19,20]) on modifications to the pipe wall (such as baffles [21,22], fins [23–30], ribs [31–36] and corrugated tubes [37–41]) or a combination of both [14]. In general, the purpose of passive techniques is to increase the heat transfer surface and enhance the convective heat transfer by altering the internal flow.

One of the most widely adopted and successful passive techniques is surface modification due to the effective heat transfer enhancement and ease of implementation in applications [32,42]. Internal helical ribs and finned tubes are among the most commonly used modification techniques that are efficient and also allow for high production rates [30,32,42]. Such high rates are particularly important for geothermal collector pipes that are typically hundreds of meters long. It is, therefore, important that the modifications are cheap and easy to manufacture, or else it is typically more economical to just drill deeper [4]. In this work, we therefore choose to explore the use of internal fins or ribs.

The effect of continuous internal fins on the pipe thermohydraulic performance has also received significant attention in previous research. See, for example, Tu et al. [30], Mousa et al. [13] and Ji et al. [42] for comprehensive overviews. However, geothermal systems pose distinct requirements, and to determine a suitable fin design, several practical aspects need consideration:

- the internal fins should be relatively straightforward to incorporate in conventional continuous plastic pipe extrusion processes. Therefore, we focus here on pipe geometries with a constant cross-section (i.e. non-intermittent fins) that, however, may rotate to some extent around the axial direction of the pipe.
- geothermal heat pumps operate at varying loads due to the fluctuating demand on hourly, daily and seasonal time scales. Many heat pumps regulate the load using inverter-controlled brine circulation pumps that effectively minimize the required average brine velocity U_b to save pump energy. This gives varying liquid flow rates and typical Reynolds numbers $Re = U_b D/\nu$ in the range

of approximately $1300 < Re < 3300$, where D is the pipe inner diameter and $\nu = \mu/\rho$ the kinematic viscosity of the brine. Within this range, the critical transition to turbulence for smooth pipes is at $Re_c \approx 2300$. Thus, the collector system is operated at both laminar and unsteady flow conditions.

- for smooth pipes with an unsteady flow ($Re > Re_c$), the convective heat transfer resistance from the pipe wall to the liquid is already small compared to the thermal resistance of the borehole (overall thermal resistance of the ground heat exchanger) [5]. An increase of the convective heat transfer rate at $Re > Re_c$ (due to the introduction of fins) does therefore not give a significant gain in the overall efficiency of the system compared to conventional smooth pipes.
- for smooth pipes with a laminar flow ($Re < Re_c$), the convective heat transfer resistance becomes a major contribution (around 50% [4]) of the total thermal resistance of the borehole. The potential for improving the overall efficiency of the geothermal system (compared to smooth pipes) is therefore highest at $Re < Re_c$.
- if the pipe friction factor f increases significantly (compared to a smooth pipe) at $Re > Re_c$ there may even be a net loss in the overall system efficiency. This is because the energy consumption of the brine circulation pump often constitutes a significant part of the total energy consumption of the heat pump, even for smooth pipes [43]. For example, the pump energy required for a 33% water-propylene glycol solution in a 600 m smooth collector pipe (32 mm inner diameter) operated at $Re = 2800$ for one year amounts to more than 1000 kWh. Here, we argue that if f increases more than about 5%–10% at $Re > Re_c$ (by adding fins) it may become, in general, difficult to claim a net gain at the system level. Moreover, the pump power requirement for a given pipe scale as $P \propto f U_b^3$ [44]. Hence, to save energy, it is important to minimize both U_b and f. By enhancing the heat transfer at $Re < Re_c$, a lower U_b can potentially be used for the same heat load. However, since f in general varies with U_b (and $P \propto U_b^3$), it is still important to maintain low f at high U_b (or high Re since $Re \propto U_b$). In addition, today, many heat pumps come with pre-installed circulation pumps specifically designed to handle pressure drops in smooth pipes. If f is then significantly increased by adding fins, there is a risk such pumps will not deliver the required flow rate.

With these considerations in mind, a suitable set of fins should thus promote the transition to an unsteady flow at $Re < Re_c$, (to significantly decrease the convective heat transfer resistance at these operating conditions) without significantly increasing the friction factor f at $Re > Re_c$. The goal of the present study is to find a fin design that achieves both of these objectives.

Although many studies have been conducted on the thermohydraulic performance of finned pipes, very few designs have been evaluated with the above-mentioned constraints. Most studies have focused on either fully turbulent or laminar conditions [16,41,42] whereas the present problem concerns Re in the transitional regime. The constraint of low f (particularly at $Re > Re_c$) also disqualifies most designs with large fins (fin sizes $O(0.1D)$) that generally induce much higher pressure drop than smaller 'micro' fins (fin sizes $O(0.01D)$) [27,42,45]. To the best of the authors' knowledge, there have not been previous studies assessing internal fins designed for the present objectives.

Numerical simulation methods for thermo-fluidic problems in complex finned geometries range from classical finite-volume/finite-element Navier–Stokes solvers to mesoscopic approaches such as the Lattice Boltzmann Method (LBM). LBM has grown in popularity for heat-transfer and conjugate heat-transfer problems [46,47] because it simplifies meshing for complex or porous geometries, is straightforward to parallelize, and can be formulated to treat fluid–solid coupling and phase change. Regardless of the method, high-fidelity DNS remains essential to provide benchmark data and mechanistic insight into near-wall turbulence and convective heat transfer. In this study, a Navier–Stokes DNS solver is employed rather than Reynolds-Averaged Navier–Stokes (RANS) or Large Eddy Simulation (LES) modelling approaches because of the inherent characteristics of transitional pipe flows. The transitional regime for heat transfer in smooth pipes (approximately $2000 < Re < 4000$ [48]) is dominated by intermittent laminar–turbulent structures (puffs) that are unsteady and spatially localized [49]. The flow regime is also highly sensitive to finite amplitude perturbations. Conventional RANS turbulence models are typically developed for statistically steady, fully turbulent flows and therefore fail to capture the intermittent dynamics and the associated heat transfer mechanisms [50,51]. Moreover, existing transition-sensitive RANS models rely on empirical correlations that are not developed for the complex fin geometries and high-Prandtl-number fluids considered here [50,52]. DNS resolves all relevant spatiotemporal scales directly, eliminating model uncertainty and provide physically consistent predictions of both hydrodynamic and thermal fields. These results further facilitate improved transition-capable turbulence models and design guidelines for finned and internally modified pipes.

In this work, we evaluate, using finite-volume DNS, the thermohydraulic performance of pipes with internal fins. The objectives of the assessment are to understand how different fin designs influence the flow and to find a promising fin design that triggers an unsteady flow at $Re < Re_c$ (to enhance the convective heat transfer) without significantly increasing the friction factor f (pressure drop) at $Re > Re_c$. Due to the high computational cost of DNS, promising fin configurations identified here are not formally optimized. The parametric analysis, however, provides clear insights into how key geometrical parameters influence performance, highlighting designs that outperform conventional smooth pipes. We start our analysis by evaluating three continuous fin design strategies; straight fins along the pipe axial direction; fins continuously rotating around the axial direction, and fins rotating in alternating directions around the axial direction. Then, we assess the influence of the fin size, the number of fins and their twist rate on the thermohydraulic performance. Based on the parameter tests, we select a promising fin design and compare the performance to that of a smooth pipe under relevant operating conditions $1300<Re<3300$ and brine Prandtl numbers $20<Pr<75$. Finally, we provide correlations for the heat transfer rate and pressure drop obtained with a promising fin design.

2. Methodology

In this paper we evaluate, using DNS, the thermohydraulic performance of pipes with and without internal fins. The DNS framework is outlined in Section 2.1 and our grid study and validation of the framework is presented in Section 2.2. We evaluate three different fin design strategies in Section 3.1. Then, the most promising design is used to study the influence of the fin size, the number of fins and their twist rate on the thermohydraulic performance in Section 3.2. This analysis provides a promising fin design that is evaluated in the entire range of relevant operating conditions and compared to the performance of a smooth pipe in Section 3.3.

Our numerical methodology starts with the following simplifying assumptions. Collector pipes are generally several hundreds of meters long while a fully developed state is typically achieved within the first 10 meters [50]. Therefore, we neglect entrance region effects and focus on evaluating the thermohydraulic performance of the collector pipes at fully developed (hydro- and thermodynamic) conditions. This allows us to use periodic boundary conditions on a representative section of the pipe, thus significantly reducing the simulated pipe length. The performance evaluation is limited to the convective heat transfer in the brine. The heat transfer in the pipe wall and the surrounding media is thus not considered here. The thermophysical properties of the working fluid are assumed constant since typical temperature variations in

geothermal collector systems rarely exceeds 5 °C, which does not cause significant changes in these properties. For indirect heat transfer systems, the key properties of secondary fluids (density, viscosity, specific heat, and thermal conductivity) vary primarily with temperature and concentration, both of which remain effectively constant in a given geothermal installation [53]. The relevant range of conditions is summarized in Table 1. The pressure drop along the collector loop (order of 10–100 kPa) is several orders of magnitude smaller than that required to produce significant density changes [54]. Polyethylene collector pipes are typically manufactured to tight standards (for example SS-EN 12201-2:2024), ensuring smooth internal surfaces and hence negligible roughness effects except where fins are introduced. We thus consider smooth wall surfaces here.

Based on these assumptions, we now present a detailed description of the numerical framework.

2.1. Numerical framework and operating conditions

We study, using Direct Numerical Simulations (DNS), fully developed flow in circular pipes, with and without surface modifications (fins), using periodic boundary conditions in the axial x-direction. The pipe in the computational domain has diameter D and length L. The wall boundary conditions are no slip $\boldsymbol{u} = 0$ and constant wall temperature $T_w > T_b$ where the bulk temperature is defined as $T_b = \frac{1}{\Omega_l}\int_{\Omega_l} T u_x d\Omega$, the Ω_l is the liquid volume and u_x is the axial velocity component.

In the remainder of this report (unless otherwise stated), all variables are made non-dimensional by the pipe diameter D, bulk velocity $U_b = \frac{1}{\Omega_l}\int_{\Omega_l} u d\Omega$ and liquid density ρ as: $x_i^* = x_i/D$, $u_i^* = u_i/U_b$, $t^* = tU_b/D$, $p^* = p/(\rho U_b^2)$. The non-dimensional temperature is defined as $T^* = (T - T_b)/(T_w - T_b)$ that gives a $T_w^* = 1$ and $T_b^* = 0$. The asterisk notation is hereafter omitted for brevity. The non-dimensional governing equations then becomes

$$\nabla \cdot \boldsymbol{u} = 0\,, \tag{1}$$

$$\frac{\partial \boldsymbol{u}}{\partial t} + (\boldsymbol{u}\cdot\nabla)\boldsymbol{u} = -\nabla p + \frac{1}{Re}\nabla\cdot(2\mu\boldsymbol{S}) + \boldsymbol{a}\,, \tag{2}$$

$$\frac{\partial T}{\partial t} + \boldsymbol{u}\cdot\nabla T = \frac{1}{RePr}\nabla^2 T + S_Q\,, \tag{3}$$

where $\boldsymbol{u}$ is the velocity, p the pressure, $\boldsymbol{S} = (\nabla\boldsymbol{u} + \nabla\boldsymbol{u}^T)/2$ the rate of deformation tensor, $\boldsymbol{a}$ is the uniform axial driving force required to maintain a constant axial flow rate, T is the liquid temperature and S_Q is the uniform cooling term required to maintain a constant bulk temperature and thus axial periodicity of the temperature field.

Because of dynamic similarity (Reynold's law of similarity), for a given pipe geometry, the present problem is completely described by specifying the Reynolds $Re = U_b D/\nu$ and Prandtl $Pr = c_p\mu/k$ numbers (where c_p is the specific heat and k is the thermal conductivity). The value of each individual parameter such as U_B or ν is thus not important but rather the ratios described by Re and Pr. This fact generalizes our method and results, making them applicable to any geometrically similar pipe flow with the same Re and Pr.

Typical material properties, operating conditions and the resulting Pr and Re values for common brines (water solutions) are given in Table 1. Here, we consider flow rates in the interval $Q = 0.1 - 0.7\ l/s$ where the lower range of the interval is obtained by many inverter-controlled heat pumps operating at low heat loads and the upper range is limited by excessively high pressure losses at higher flow rates. The material properties are evaluated at 0 °C which is the conventional design operating temperature of VGHEs. Lower operating temperatures are preferably avoided to minimize the risk of ground water freezing and damage to the system while higher temperatures requires deeper or more boreholes for the same heat load.

Table 1 indicates that the relevant ranges of the governing parameters are approximately $400 < Re < 7000$ and $20 < Pr < 75$. However, as discussed in Section 1, our primary objective in introducing fins is to induce unsteady flow at $Re < Re_c$, thereby significantly enhancing heat transfer under conditions where conventional smooth pipes remain laminar, without causing a substantial increase in the friction factor f at $Re > Re_c$. Accordingly, we focus on the interval $1300 \le Re \le 3300$, where a finned design is expected to trigger unsteady flow. At Re below this range, any practical fin design will most likely result in laminar flow, while at Re well above Re_c, the flow is fully turbulent and smooth pipes already provide high heat transfer. This interval also allows us to evaluate the increase in pressure drop under conditions where both smooth and finned designs exhibit turbulent flow.

The governing equations Eqs. (1)–(3) are solved using the open-source code Basilisk (basilisk.fr) [55] where the geometry is parametrised and defined using the embedded boundary method [56] and constructive solid geometry operations. The code features a second-order finite volume solver and Cartesian tree-based grid structure that allows for automatic geometry/grid generation and efficient solution of the governing equations. The tree-based grid structure is based on cubic cells that are suitable for the present study where the grid should resolve relatively complex and small surface modifications. This would not be possible with cells elongated in the streamwise direction (to reduce the number of cells) which is typical in DNS of wall-bounded turbulence on smooth surfaces.

The non-dimensional bulk velocity $U_b = 1$ is forced by applying a time-dependent but spatially uniform acceleration term a_x in Eq. (2) (determined using a PI-controller). At steady flow conditions, the total forcing $F_a = \Omega_l \rho a_x$ exactly balances the wall shear stress $F_w = \tau_w \pi D L$. The equivalent pressure drop over the pipe is $F_a = \pi(D/2)^2\Delta p$ that gives $\Delta p/L = \rho a_x$ (assuming the total liquid volume $\Omega_l = \pi(D/2)^2 L$ is approximately correct even with surface modifications). Defining the pipe friction factor f as $\Delta p = f(L/D)(\rho U_b^2/2)$ then gives $f = 2a_x D/U_b^2$.

The same forcing methodology (as for U_b) is used in the energy equation Eq. (3) where S_Q is varied uniformly (with another PI-controller) to force $T_b = 0$, similarly to the methodology of Pirozzoli et al. [57]. At statistically steady conditions, the total cooling rate $Q_c = \Omega_l S_Q$ equals the total wall heat flux $Q_w = q_w \pi D L$. The wall heat flux is thus $q_w = S_Q D/4$. With the convective heat transfer coefficient $h = q_w/(T_w - T_b)$ we further define the non-dimensional Nusselt-number as $Nu = hD/k$ that represents the ratio of convective to conductive heat transfer.

For a fully developed laminar flow with $U_b = 1$ in smooth circular pipes of radius $R = D/2$, the axial velocity profile is $u_x(r) = 2(1 - (r/R)^2)$, where r is the radial coordinate from the pipe centre. With the uniform cooling term S_Q balancing the heat flux, the temperature profile is constant in the axial direction and the energy equation in polar coordinates reduces to

$$\frac{1}{RePr}\frac{1}{r}\frac{\partial}{\partial r}\left(r\frac{\partial T}{\partial r}\right) = -S_Q\,. \tag{4}$$

The radial temperature profile $T(r) = RePr\frac{S_Q}{4}(R^2 - r^2) + 1$ can then be obtained by integrating twice and applying the boundary conditions $T(R)=1$ and $\partial T/\partial r(r=0)=0$. By further imposing $T_b = \frac{1}{\pi R^2}\int_0^R T(r)u_x(r)\,2\pi r dr = 0$ and inserting the expression for $T(r)$, we can solve for $S_Q = -6/(R^2 RePr)$. The latter result gives a theoretical $Nu_{smooth,lam} = 6$ for laminar flow in smooth pipes with our numerical approach. This is thus the lower limit of Nu that we should expect from the simulations.

It should be noted that $Nu_{smooth,lam} = 6$ deviates from the classical result $Nu \approx 3.66$ valid for smooth pipes with laminar flow and a constant wall temperature without any cooling term. In the latter case, the bulk temperature asymptotically approaches the wall temperature along the axial direction of the pipe, and it would not be straightforward to use standard periodic axial boundary conditions. Because of the high computational cost of DNS, the use of a relatively short periodic domain is necessary. Nevertheless, our approach gives heat transfer rates that remain suitable for relative comparison but are also close

Table 1
Typical material parameters and operating conditions for common brines (water solutions) used in geothermal heat collector systems [53]. All values are calculated at the conventional lower operating temperature of 0 °C. To calculate Re, we use a pipe diameter of $D = 40$ mm and typical flow rates in the interval $Q = 0.1$–0.7 l/s.

Brine	C_A [wt-%[	ρ [kg/m^3]	c_p [J/(kgK)]	k [W/(mK)]	μ [mPas]	Pr [–]	Re [–]
Ethylene glycol	30	1046	3677	0.447	4.31	36	771–5400
Potassium carbonate	30	1307	2932	0.536	4.29	23	970–6790
Propylene glycol	33	1035	3852	0.416	8.17	76	403–2820
Ethanol	29	967	4193	0.403	6.40	67	481–3365

to experimental correlations and cases without the cooling term in the unsteady flow regime [57].

The transition to turbulence for a smooth pipe typically occurs at about $Re_c = 2300$, but the exact value may vary in the range of approximately $2000 < Re < 4000$ depending on inlet/initial conditions, wall roughness or other flow disturbances. In real geothermal collector systems, we anticipate significant disturbances by the recirculation pump, wall defects, pipe bends etc. and to mimic these conditions, we simulate all designs first at $Re = 3300$ or $Re = 2300$ where the flow always becomes turbulent. Then, we successively lower Re in the discrete steps of $Re = (3300, 2300, 2050, 1950, 1800, 1700, 1300)$. For each reduction, we let the flow reach a statistically steady state (where all relevant statistics regarding the hydro- and thermodynamics, such as the time-averaged friction factor and the heat transfer coefficient, are constant in time) before we reduce Re further. This approach ensures that the initial conditions for a specific geometry and Re are always a relevant unsteady flow solution until a laminar solution is reached (all velocity fluctuations are dampened). The results from each simulation case are time-averaged during fully developed conditions until the values are practically independent of the averaging period.

2.2. Grid study and validation

Here, we assess whether our numerical grid resolves all relevant scales, that the results are grid convergent and that the results agree with experimental correlations in the relevant range of operating conditions.

We start by examining the required grid resolution to resolve all relevant scales of the flow. The value of $Re = 3300$ gives the smallest turbulent scales and is thus most challenging from a numerical perspective. Therefore, this value is chosen as our test case. We also choose a smooth pipe so that we can compare our results with available correlations from the literature. Our base grid, shown in Fig. 1(a), consists of cubic cells with the side length $\Delta = D/58$ in the pipe core and with a refinement region of about 10 cells at the wall with $\Delta = D/116$. This gives an $y^+ = yu_\tau/\nu \approx 1$ (where $u_\tau = \sqrt{\tau_w/\rho}$) for the cell closest to the wall, which is a requirement for DNS of wall-bounded turbulence. We also get a ratio of $\Delta/\eta = 1.4$ in the near-wall region (where the Kolmogorov length scale is $\eta = (\nu^3/\varepsilon)^{(1/4)}$ and the dissipation rate equals the power input per unit mass $\varepsilon = U_b a_x$). This ratio is below the DNS resolution criterion of Pope [58] ($\Delta/\eta \lessapprox 2.1$) for isotropic turbulence and should thus sufficiently resolve the smallest velocity scales.

Since $Pr \gg 1$ in the present study, we may however expect even smaller thermal scales, especially close to the wall. To assess the effect of this, we add another refinement level of about 10 cells with $\Delta = D/232$ at the wall, shown in Fig. 1(b) for the most demanding case of $Re = 3300$ and $Pr = 75$. Here, we note that although some small-scale thermal regions are likely under-resolved, the boundary layer thickness and the flow characteristics are qualitatively the same for both resolutions. This indicates that the base grid is sufficient to capture the governing heat transfer processes. The effect of the grid resolution on the results is also quantified as follows. Fig. 2(a) shows the friction

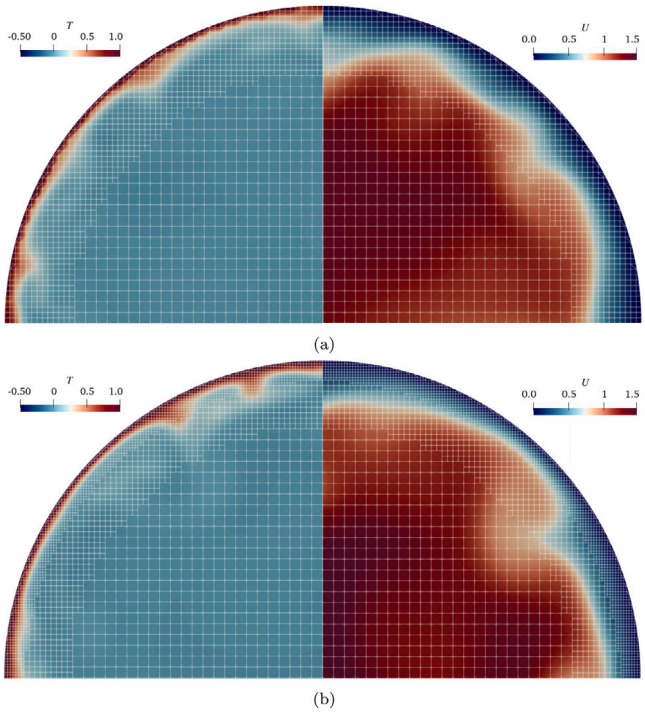

Fig. 1. (a): Base grid (white lines) of $\Delta = D/58$ in the core and $\Delta = D/116$ at the near-wall region. (b): Refined grid with an additional refinement region of $\Delta = D/232$ closest to the wall. The colour contours in the left and right half represent the non-dimensional temperature and velocity magnitude, respectively, for the case $Re = 3300$ and $Pr = 75$. (For interpretation of the references to colour in this figure legend, the reader is referred to the web version of this article.)

factor f for the base and the refined grid, together with the correlation of Haaland [59] for turbulent pipe flows given by

$$\frac{1}{\sqrt{f}} = -1.8 \log_{10}\left[\left(\frac{\varepsilon/D}{3.7}\right)^{1.11} + \frac{6.9}{Re}\right] \tag{5}$$

where we use the value $\varepsilon/D = 10^{-5}$ corresponding to smooth pipes. We observe excellent agreement with the correlation for both grids and a relative difference of only 1% with the refined grid. Fig. 2(b) shows the predicted Nu for the cases of $Pr = (20, 40, 75)$ and the corresponding Gnielinski [60] and Meyer et al. [61] correlations for turbulent (and quasi-turbulent [61]) flow in pipes expressed as

$$Nu_{Gni} = \frac{(f/8)(Re - 1000)Pr}{1 + 12.7\sqrt{f/8}(Pr^{2/3} - 1)}, \tag{6}$$

$$Nu_{Meyer} = 0.041 Re^{1.117} Pr^{1/3} f. \tag{7}$$

In Fig. 2(b), we observe fair agreement with the correlations and the correct increase of Nu with Pr. The relative difference using the refined grid increases slightly with Pr as 0% at $Pr = 20$, 1% at $Pr = 40$

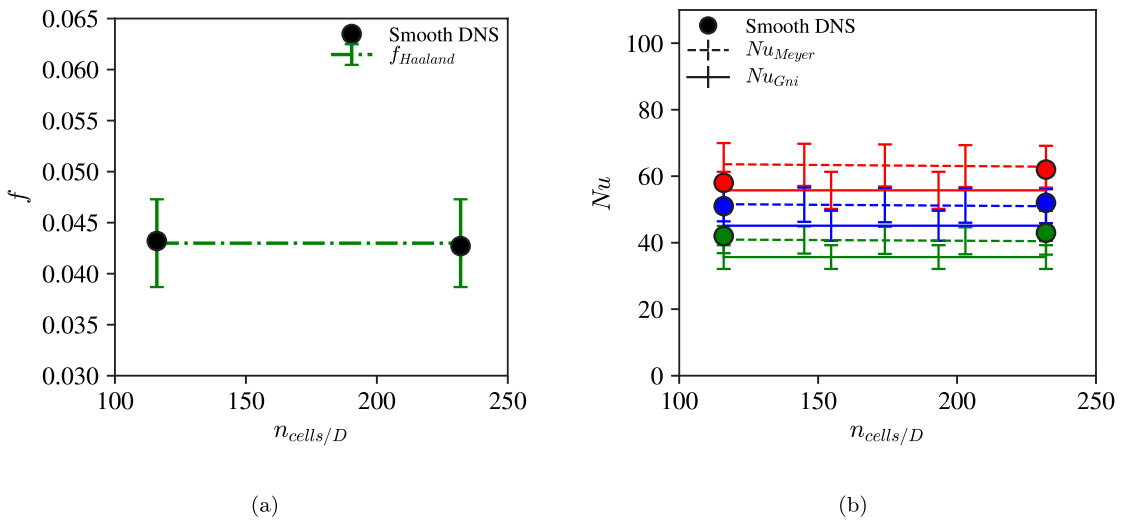

Fig. 2. Grid dependency study for a smooth pipe with $Re = 3300$ and $Pr = (75, 40, 20)$. (a): Predicted friction factor and comparison to by Haaland Eq. (5) ±10%. Here we observe a relative difference of only 1% with the refined grid and an excellent agreement with the correlation. (b): Predicted Nu and comparison to the correlations Eq. (6) and Eq. (7) ±10% evaluated using f from our DNS at the corresponding resolution. The red, blue and green colours represent cases with $Pr = (75, 40, 20)$, respectively. The relative difference between the refined grid to the base grid is 6% or less for all cases where we observe fair agreement with the correlations. (For interpretation of the references to colour in this figure legend, the reader is referred to the web version of this article.)

and 6% for $Pr = 75$. Considering that the case $Re = 3300$ and $Pr = 75$ constitutes the most numerically challenging parameter set in this study, the relative error of using the base grid should be about 5% or less for all other cases. This is deemed sufficient for the present study where the main focus is on studying the effect of internal fins on the hydrodynamics. The base grid resolution gives more than 26×10^6 grid points for the cases with $L = 35D$ that are typically simulated for $tU_b/D = 500 - 1000$ time units to get converged time-averaged results. This highlights the large computational costs of the DNS performed in the present work.

Next, we use our base grid to simulate the flow and heat transfer rate for the entire relevant range of operating conditions ($1300 < Re < 3300$ and $20 < Pr < 75$). The simulations start at $Re = 3300$ and then Re is successively reduced (after a statistically steady state is reached) until $Re = 1300$. The transition from a laminar to a turbulent flow in a smooth pipe generally occurs at the critical value $Re_c = 2300$. The validation cases thus assess whether our DNS predict the turbulent transition correctly and if the predicted f and Nu quantitatively agree with analytical solutions for laminar flow ($f = 64/Re$ and $Nu_{smooth,lam} = 6$) and experimental correlations in the turbulent regime (Eqs. (5)–(7)). The parameters used for the validation cases are tabulated in Table 2 and the DNS results are shown in Fig. 3. In Fig. 3(a), we observe an excellent agreement with both analytical solutions and experimental correlations and that the turbulent transition is indeed predicted close to $Re_c = 2300$. Fig. 3(b) also shows good agreement and that we capture the turbulent transition at Re_c. We acknowledge however, that the turbulent heat transfer correlations are generally less accurate at the relatively low ($Re \lessapprox 4000$) considered here due to the inherently unstable and intermittent flow behaviour. Therefore, a deviation of approximately 20% is generally to be expected [61]. Our DNS results are within these error margins for all parameters relevant to the present study. The validation cases thus confirm the accuracy of our numerical setup and the ability of the DNS to accurately capture the complex flow instabilities leading to the turbulent transition. The numerical setup and the base grid of Fig. 1(a) are consequently used in all subsequent simulations.

The DNS predictions of Nu for finned pipes are compared with the Eq. (7) in Fig. 10(b), which provides a general correlation applicable to both smooth and rough tubes [61]. The fin geometries in this study feature small protrusions designed to maintain low f, effectively resembling a rough surface, making Eq. (7) a suitable reference. The results show good agreement, with deviations within 7% for all cases exhibiting unsteady flow at $Re \geq 1950$, confirming that the DNS accurately captures the heat transfer behaviour and aligns with established empirical trends.

Table 2
Nondimensional parameters used for the validation of our numerical framework. The DNS simulations are performed in a smooth periodic pipe of $L = 8.8D$ using our base grid size. For this setup, we can compare the predicted f and Nu against both analytical (laminar flow with $f_{lam} = 64/Re$ and $Nu_{smooth,lam} = 6$) and experimental correlations (turbulent (and quasi-turbulent [61]) flow with $f_{Haaland}$ (Eq. (5)), Nu_{Gni} (Eq. (6)) and Nu_{Meyer} (Eq. (7)). Here, we evaluate Nu_{Gni} and Nu_{Meyer} using the friction factor from $f_{Haaland}$. The simulations span the turbulence transition region starting at $Re = 3300$ and then Re is successively reduced (after a statistically steady state is reached) until $Re = 1300$. We note a good overall agreement between our DNS and the correlations with values for Nu_{DNS} at $Re \geq 2300$ between the predictions by the experimental correlations. These results are further presented graphically in Fig. 3.

Re	Pr	f_{DNS}	f_{lam}	$f_{Haaland}$	Nu_{DNS}	Nu_{lam}	Nu_{Gni}	Nu_{Meyer}
3300	75	0.0432		0.0430	58		56	63
2300	75	0.0472		0.0485	42		34	48
2050	75	0.0311	0.0312		6	6		
1800	75	0.0353	0.0355		6	6		
1300	75	0.0489	0.0492		6	6		
3300	20	0.0432		0.0430	42		36	41
2300	20	0.0472		0.0485	29		22	31
2050	20	0.0311	0.0312		6	6		
1800	20	0.0353	0.0355		6	6		
300	20	0.0489	0.0492		6	6		

3. Results

We start by evaluating three fin design strategies in Section 3.1 and then focus on the most promising design to assess the influence of the fin size, the number of fins and their twist rate on the heat transfer rate and pressure drop in Section 3.2. Then, we compare the thermohydraulic performance of a specific promising fin design with a smooth pipe in Section 3.3, evaluate a performance evaluation criterion (PEC) for this design in Section 3.3.1 and develop a regression model for the heat transfer rate and the pipe friction factor based on our DNS in Section 3.4.

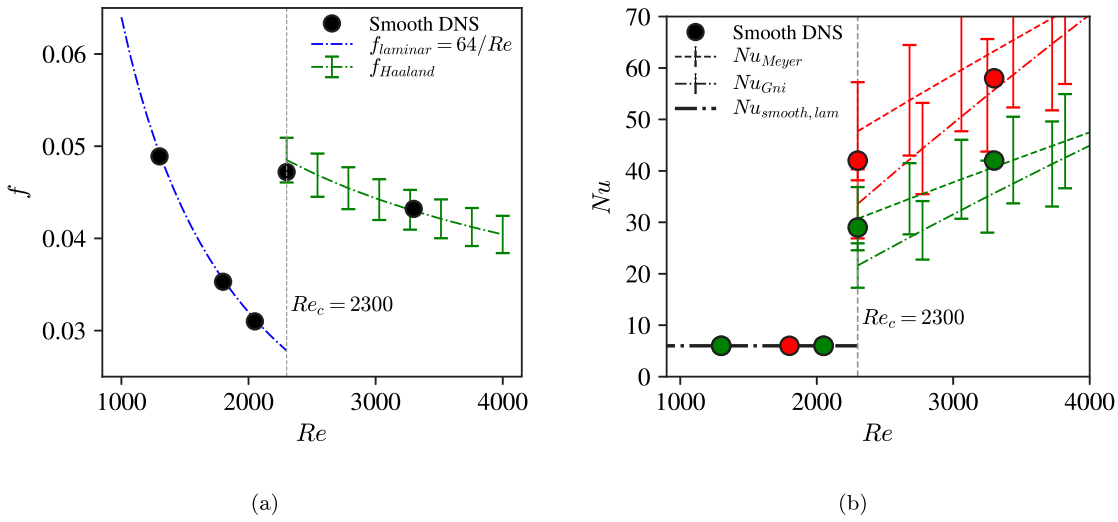

Fig. 3. Validation of (a): the predicted friction factor f and (b): the predicted heat transfer rate Nu for a smooth pipe in the turbulence transition region of $1300 \leq Re \leq 3300$. The transition from a laminar to a turbulent flow in a smooth pipe generally occurs at the critical value $Re_c = 2300$. In (a), we compare our DNS predictions to the analytical solution $f = 64/Re$ for laminar flow and the experimental correlation by Haaland Eq. (5) ±10% for turbulent pipe flow. The results show an excellent agreement for both laminar and turbulent flow, confirming that the turbulent transition is accurately captured in our numerical framework. In (b), we compare our DNS to the analytical solution $Nu = 6$ for laminar flow with a uniform cooling term and the experimental correlations Eq. (6) and Eq. (7) ±20% for turbulent pipe flow evaluated using Eq. (5). The red and green colours represents cases with $Pr = 75$ and 20, respectively. Here, we also observe a good agreement at laminar and turbulent flow conditions. The turbulent heat transfer correlations are however generally less accurate at the relatively low ($Re \lessapprox 4000$) considered here due to the inherently unstable and intermittent flow behaviour. Consequently, a deviation of about 10%–20% is generally to be expected [61]. (For interpretation of the references to colour in this figure legend, the reader is referred to the web version of this article.)

3.1. Evaluation of different fin design strategies

Apart from increasing the convection surface area, the main purpose of most fin designs is to enhance the convection coefficient by increasing the mixing of the momentum and thermal wall boundary layers. This is generally achieved by disrupting the flow such that higher velocity liquid is brought closer to the wall [62]. The near-wall velocity can be increased either directly by forcing the near-wall flow in, for example, a tangential direction or indirectly by, for example, locally triggering an unsteady (or even turbulent) separated flow that propagates downstream with the bulk flow [42]. In the direct approach, the fin heights typically need to be comparable to the momentum boundary layer thickness or greater to significantly enhance the near-wall velocity. Such large fins may however also increase the pressure drop significantly. With the indirect approach, the fin sizes can be smaller as long as the disturbances cause sufficiently unsteady separated flow regions to enhance the heat transfer. The latter approach thus also requires sufficiently low viscous forces so that the fin-induced disturbances are not directly dissipated.

Since geothermal collector systems generally operate close to Re_c (and low pressure drop is important) we focus on investigating relatively small fins with the aim of triggering separated unsteady flow at $Re < Re_c$, without significantly increasing the friction factor f at $Re > Re_c$.

However, in general, any fin design increases f [42]. To minimize this effect, we focus on fin designs aligned mainly in the flow direction since fins oriented perpendicular to the flow direction are more likely to significantly increase f.

Three fin design strategies are evaluated; straight fins aligned with the pipe axis; fins arranged in a continuous helical pattern about the pipe axis; and fins with alternating helical orientations along the pipe axis. Illustrations of these designs (one full period of the fins in the axial direction) are shown in Fig. 4. Here, we have chosen a number of fins $n_{fin} = 16$ with equal circumferential spacing, a height of $h_{fin}/D = 0.015$ and a base width of about $2h_{fin}$ for all fin designs. These values were identified as relevant through a review of existing finned collector tube designs in the industry. We also performed preliminary numerical tests to confirm that such parameters typically give insignificantly higher f at $Re > Re_c$ but may still trigger an unsteady flow at $Re < Re_c$. The chosen parameters thus provide a good starting point for further exploration.

The fin cross-section is shown schematically in Fig. 5(a) and an illustration of the inner pipe wall for the alternating helical fin design is shown in Fig. 5(b) together with the non-dimensional temperature field for the case $Re = 2300$, $Pr = 75$. Here, the fins with $h_{fin}/D = 0.015$ still appear smaller than the thermal boundary layer thickness. Since the thermal boundary layer is thinner than the velocity boundary layer, it is reasonable that the effect of these fins on the pressure drop should be small. The effect of larger fins is assessed in Section 3.2.1.

The pipe length is $L = 8.8D$ for the straight fins, $L = 17.5D$ for the continuously helical fins and $L = 35D$ for the fins with alternating helical orientations. These lengths give the same fin twist rate $\omega_{fin} = 360°$ (one revolution in about $17.5D$) in the continuous and alternating helical configurations. The shorter length for the straight fins is chosen to reduce the computational cost but still capture the relevant length scales of the unsteady flow. Please note that Fig. 4(c) is compressed to $L = 17.5D$ in the axial direction for visualization purposes. For reference, a typical pipe inner diameter is about $D = 40$ mm that gives $h_{fin} = 0.015D = 0.6$ mm and $L = 35D = 1.4$ m.

The simulations are started at $Re = 2300$ where all designs exhibit an unsteady flow. The Re is then successively lowered until the flow becomes laminar (velocity fluctuations decay to negligible levels and Nu and f approach the laminar analytical solutions). For the laminar cases, the Nu exhibits very slow convergence towards a value between 6 and 7 where the exact value is not deemed important at this stage. It is however reasonable that Nu is slightly above $Nu_{smooth,lam} = 6$ (derived for smooth pipes with laminar flow in Section 2.1) since the fins increase the heat transfer area and still induce an altered flow (especially close to the wall) compared to the smooth pipe. The results from the simulations are presented in Table 3 where it is clear that the flow becomes laminar at $Re = 2050$ for the straight fins, $Re = 1950$ for the continuous helical fins and $Re = 1700$ for the alternating helical fin

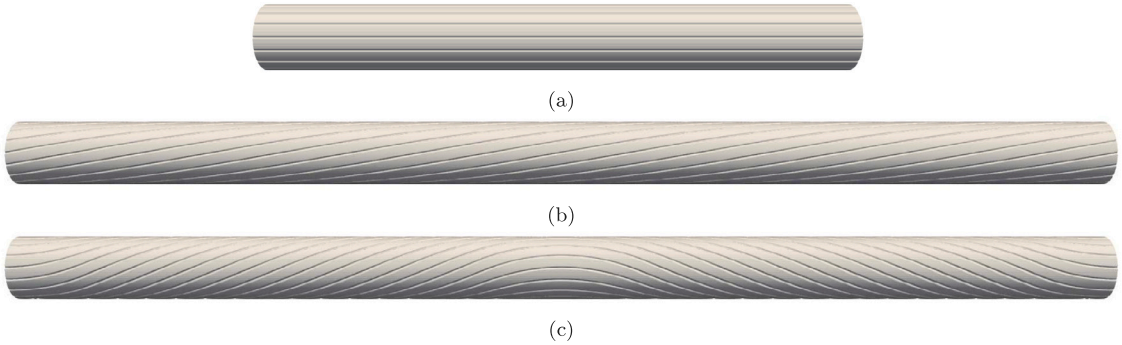

Fig. 4. Illustration of the three evaluated fin design strategies (inner pipe wall surface). (a) Straight fins aligned with the pipe axis, $L = 8.8D$. (b) Fins arranged in a continuous helical pattern (one full revolution in $L = 17.5D$). (c) Alternating helical fins along the pipe axis with one full revolution in both directions during $L = 35D$ (here the pipe is compressed to half its actual length for visualization purposes). With a typical pipe diameter of $D = 40$ mm, the simulated lengths corresponds to 0.22 m, 0.7 m and 1.4 m, respectively.

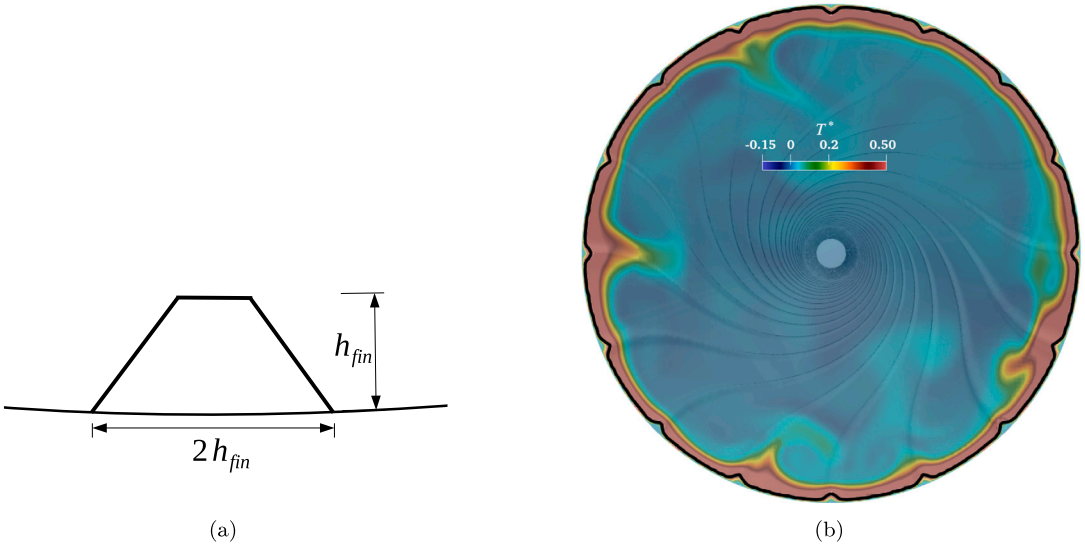

Fig. 5. (a) Schematic illustration of the fin cross-section that is used in all evaluated fin designs. (b) Inner pipe wall surface with the alternating helical fin design and $h_{fin}/D = 0.015$ (viewed in the pipe axial direction) constructed using the embedded boundary method. The black line indicates the inner pipe surface at the pipe cross-section $x = 0$ and the transparent colour contours represent the non-dimensional temperature field for the case $Re = 2300$ and $Pr = 75$. (For interpretation of the references to colour in this figure legend, the reader is referred to the web version of this article.)

Table 3
Time-averaged DNS results for $Pr = 75$ and various Re in the evaluation of the straight, continuous helical and alternating helical fin designs shown in Fig. 4. The simulations are started at $Re = 2300$ where all designs show an unsteady flow and then Re is successively lowered until the flow becomes laminar.

	Straight			Continuous			Alternating		
Re	Nu	f	Flow type	Nu	f	Flow type	Nu	f	Flow type
2300	43	0.0471	unsteady	44	0.0477	unsteady	43	0.0474	unsteady
2050	6–7	0.032	laminar	34	0.0435	unsteady	33	0.0414	unsteady
1950	–	–	–	6–7	0.0332	laminar	30	0.0394	unsteady
1800	–	–	–	–	–	–	26	0.0414	unsteady
1700	–	–	–	–	–	–	6–7	0.038	laminar

design. These results suggest that the alternating helical fin design can trigger an unsteady flow at significantly lower Re than the other two designs while the friction factor is practically the same at $Re = 2300$ for all designs. We also observe Nu for the unsteady flow cases that are 5–6 times those of the laminar flow cases at the same Re. Consequently, we choose the alternating helical fin design to further assess the influence of the fin size, number of fins and fin twist rate on the thermohydraulic performance.

3.2. Influence of fin parameters

Here, we evaluate the influence of the fin size, number of fins and fin twist rate for the alternating helical fin design on the thermohydraulic performance.

3.2.1. Influence of fin height

The influence of the fin height h_{fin} on f is evaluated at the operating conditions $Re = 3300$ and $Pr = 75$ where the flow is turbulent for

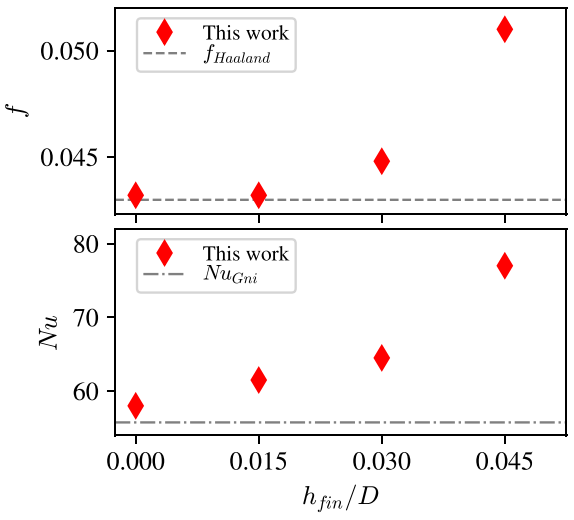

Fig. 6. Friction factor and Nusselt numbers from our DNS for different fin heights h_{fin} of the alternating helical fin design at $Re = 3300$ and $Pr = 75$. The case with $h_{fin} = 0$ represents our DNS of the smooth surface that approaches the friction factor correlation by Haaland [59] in the top panel and the heat transfer correlation by Gnielinski [60] in the bottom panel that are both developed for turbulent flows in smooth pipes.

all cases. The simulation results are shown in Fig. 6 together with the experimental correlations by Haaland [59] for f and Gnielinski [60] for Nu, where both correlations are developed for turbulent flow in smooth pipes. Here, we observe that for $h_{fin} = 0$, the simulation results converge towards the values predicted by the correlations. In the top panel, the friction factor starts to increase rapidly at around $h_{fin}/D = 0.025$, reaching a value 18% higher than the smooth surface at $h_{fin}/D = 0.045$. The Nu show a similar trend with a value almost 33% higher than the smooth surface at $h_{fin}/D = 0.045$. Based on these results, a non-dimensional fin height of around $0.015 - 0.025$ is considered a suitable choice concerning the friction factor. Consequently, an alternating helical fin design with the ratio h_{fin}/D within this interval should not have a significantly higher f than that of a smooth pipe regardless of the actual fin height or pipe diameter. In the remainder of this work, we use a $h_{fin}/D = 0.015$ where f is not expected to increase significantly at $Re > Re_c$ for any of the other fin parameters that are evaluated next.

3.2.2. Influence of the number of fins

Now, we look at how the number of fins affects the ability of the fins to induce an unsteady flow at $Re < Re_c$. Here, we again use the alternating helical fin design with a total domain length of $L = 35D$ and a $h_{fin}/D = 0.015$ but vary the number of fins n_{fin} and maintain an equal circumferential spacing. Clearly, as $n_{fin} \to \infty$ or $n_{fin} = 0$, the geometry converges to that of a smooth pipe wall. There should thus be a finite optimal value of n_{fin}. We test the values of $n_{fin} = (2, 16, 24, 32)$, starting again (for each case) with $Re = 2300$ and then successively lower the Re until a laminar flow is obtained. Before each reduction of Re, we let the simulation run sufficiently long for the flow to become statistically steady (time-averaged statistics such as f and Nu become constant in time).

The results are shown in Table 4 and suggest that around $n_{fin} > 16$ is not advantageous to induce unsteady flows at $Re < Re_c$. Interestingly, already $n_{fin} = 2$ significantly alters the flow compared to a smooth pipe (that typically transitions to a laminar flow at $Re < 2300$). The findings thus indicate that $n_{fin} \lessapprox 16$ is a suitable choice with respect to inducing an unsteady flow at $Re < Re_c$. The Nu and f-values for all unsteady cases in Table 4 are all close to (within a few per cent) the corresponding cases for the alternating design presented in Table 3 with $n_{fin} = 16$. This highlights that the main effect of the fins on the heat transfer rate is not the increased heat transfer area (that increases proportional to n_{fin}) but rather to induce an unsteady flow.

Table 4
Statistically steady (fully developed) flow type observed for various Re and number of equally spaced fins n_{fin} for the alternating helical fin design. The simulations are started at $Re = 2300$, where all designs show an unsteady flow, and then Re is successively reduced until the flow becomes laminar.

Re	$n_{fin} = 2$	$n_{fin} = 16$	$n_{fin} = 24$	$n_{fin} = 32$
2300	unsteady	unsteady	unsteady	unsteady
2050	unsteady	unsteady	unsteady	unsteady
1950	unsteady	unsteady	unsteady	laminar
1800	unsteady	unsteady	laminar	–
1700	laminar	laminar	–	–

Table 5
Statistically steady (fully developed) flow type observed for different Re and fin twisting rates ω_{fin} for the alternating helical fin design. The simulations are started at $Re = 2300$, where all designs show an unsteady flow, and then Re is successively reduced until the flow becomes laminar.

Re	$\omega_{fin} = 0°$	$\omega_{fin} = 30°$	$\omega_{fin} = 45°$	$\omega_{fin} = 180°$	$\omega_{fin} = 360°$
2300	unsteady	unsteady	unsteady	unsteady	unsteady
2050	laminar	unsteady	unsteady	unsteady	unsteady
1950	–	unsteady	unsteady	unsteady	unsteady
1800	–	laminar	unsteady	unsteady	unsteady
1700	–	–	laminar	laminar	laminar

3.2.3. Influence of fin twist rate

Finally, we evaluate how the twist rate of the fins in the alternating helical design influences the ability to induce unsteady flows at $Re < Re_c$. Here, we fix the geometry parameters $L = 35D$, $h_{fin}/D = 0.015$, $n_{fin} = 16$ but vary the twist rate of the helical parts. The twist rate is varied so that the fins rotate ω_{fin} degrees around the pipe axis in the clockwise direction during $0 \le x < L/2$ and then the same degree back in the counter-clockwise direction at $L/2 \le x \le L$. The investigated twist rates are $\omega_{fin} = (30°, 45°, 180°, 360°)$ and their influence on the flow behaviour at $Re \le Re_c$ is shown in Table 5. For reference, we also include the case $\omega_{fin} = 0°$ that equals the straight fin design evaluated in Table 3. The findings suggest that a twist rate of approximately $\omega_{fin} \gtrsim 45°$ is sufficient to induce an unsteady flow down to the region $1700 < Re < 1800$. This is the same transition region as for the case with a full fin revolution, $\omega_{fin} = 360°$. However, for $\omega_{fin} = 30°$, the effectiveness of the alternating helical fin design to induce an unsteady flow starts to decrease towards the straight fin design, $\omega_{fin} = 0°$, that gives a laminar flow already at $2050 < Re < 2300$.

In conclusion, our parameter investigations indicate that a suitable fin design can be constructed with alternating helical fins of $h_{fin}/D = 0.015$, $n_{fin} = 16$ and $\omega_{fin} = 360°$.

3.3. Thermohydraulic performance of the alternating helical fin design compared to smooth pipes

Here, we compare our promising design of alternating helical fins with $L = 35D$, $h_{fin}/D = 0.015$, $n_{fin} = 16$ and $\omega_{fin} = 360°$ to our DNS of smooth pipes ($L = 8.8D$) and available experimental correlations for smooth pipes. We evaluate three different $Pr = (20, 40, 75)$ at the operating conditions $Re = (3300, 2300, 2050, 1950, 1800, 1700, 1300)$.

Non-dimensional temperature contours (at the plane $z = 0$) for the smooth pipe DNS at fully developed conditions are shown in Fig. 7 Here, the unsteady flow at $Re = 3300$ and 2300 induces significant thermal mixing along the entire pipe axis. The mixing tend to homogenize the temperature field in the pipe core and gives relatively thin thermal boundary layers at the pipe wall. Conversely, at $Re \le 2050$, the flow becomes laminar and the heat is only transported by diffusion in the wall-normal direction, producing significantly thicker thermal

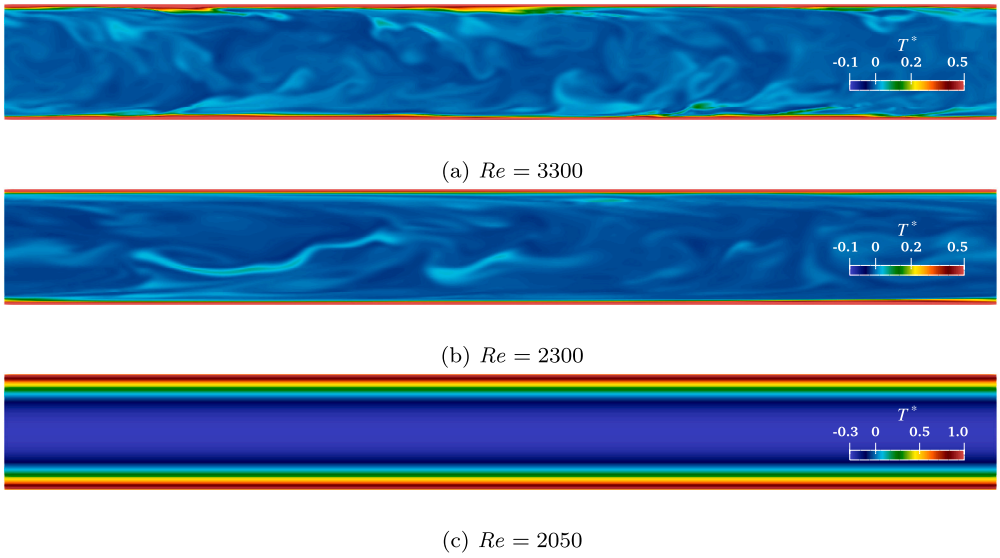

Fig. 7. Non-dimensional temperature contours at a cross-section ($z = 0$) of the smooth pipe for $Pr = 75$. The Re decreases from 3300 down to 2050, where the flow becomes laminar. The solutions for $Re < 2050$ are the same as $Re = 2050$ since the flow is laminar.

boundary layers. Fig. 8 shows the same views for the alternating helical fin design. Here, the flow is unsteady until $Re = 1700$ where the flow becomes laminar. However, at $Re \leq 2050$, the fins induce locally unsteady regions along the pipe axis. Although these unsteady regions are localized, they are advected with the flow (at approximately the bulk velocity) and disrupt the thermal boundary layer as they pass by, hence significantly enhancing the local convective heat transfer rate. These unsteady regions are likely caused by the change in the rotational direction of the fins. This is because the angular momentum (swirl) generated by the fins upstream of the fin's bend (change of rotational direction) triggers flow separation as the fins relatively abruptly bends into the other rotational direction.

This effect is illustrated in Fig. 9 that shows several instantaneous fields for the case with alternating helical fin at $Re = 2050$ (same case and instant as in Fig. 8(c)). Here, the fins bend (change rotational direction) in the beginning/end and in the middle of the periodic domain. Fig. 9(a) shows the cross-stream velocity u_z, Fig. 9(b) the axial vorticity $\omega_x = \partial u_z/\partial y - \partial u_y/\partial z$, Fig. 9(c) the temperature field and the iso-surfaces for the Q-criterion ($Q = 1/2[tr(\nabla \boldsymbol{u})^2 - tr(\nabla \boldsymbol{u} \cdot \nabla \boldsymbol{u})]$) and Fig. 9(d) contours of the local $Nu(\boldsymbol{x}, t)$ at the inner pipe wall. In Fig. 9 and Fig. 9(b), both u_z and ω_x change sign close to the pipe wall at either side of the middle bend. This is because the fins force the flow to follow their rotational direction (compare for up- and downstream the centre of the domain). At the fin bend, the swirl in the upstream region causes the flow to separate from the wall rather than to follow the fins in the opposite rotational direction. As the separated flow propagates downstream, it interacts with the fluid at the wall that is now forced to swirl in the opposite direction. This interaction is further amplified at the next fin bend (beginning/end of the domain) that leads to yet another flow separation and a chaotic flow region with intense mixing. Fig. 9(c) shows iso-surfaces for the Q-criterion that represent coherent 3D vortical structures induced by the flow separation and the swirl generated by the fins. Just after the passage of these coherent structures, we note significant disruptions of the thermal boundary layer at the wall (left side of the domain in Fig. 9(c)). These disruptions bring colder liquid towards the wall and significantly increase the local wall heat transfer rates. This is corroborated in Fig. 9(d) where $Nu(\boldsymbol{x}, t)$ show significant peaks (about double that of the average $Nu = 33$ for this case) in the same region as the thermal boundary layer disruptions. The effects of these observations on the average thermohydraulic performance are quantified next.

Fig. 10(a) shows the friction factor for all cases together with the laminar solution $f_{laminar} = 64/Re$ and the correlation by [59]. We observe an excellent agreement with the laminar solution and the correlation for the smooth pipes, further validating our numerical approach. However, for the alternating fin design, a transition to an unsteady flow (departure from the laminar solution) is observed already at about $1700 < Re < 1800$ in contrast to the smooth pipe that transitions somewhere between $2050 < Re < 2300$. The results also show that the friction factor for the alternating fin design is practically the same as that of the smooth pipe outside of the intermediate region $1700 < Re < 2300$. Specifically, the largest difference outside of this region is found at $Re = 1300$ where f for the alternating fin design is 2% higher than that of the smooth pipe. At these low Re, the pipe pressure drop is however already low. At higher $Re \geq 2300$, this difference is only about 0.4% or less.

The earlier transition to an unsteady flow using the alternating fin design is also seen in Fig. 10(b) that shows significantly higher heat transfer rates (about $300 - 600\%$ higher than the smooth pipe) in the intermediate region of about $1700 < Re < 2300$. At $Re \leq 1700$, both geometries are close to the laminar solution for a smooth pipe ($Nu_{smooth,lam} = 6$) although the alternating fin design consistently gives about $1 - 8\%$ higher heat transfer rates here. At $Re \geq 2300$, we observe no significant differences between the geometries (maximum 5% higher Nu for the alternating fin design that is about the expected accuracy at these high Re). Interestingly, using f from our DNS of the alternating fin design in the correlation by Meyer et al. [61] Eq. (7) gives Nu close to those of our DNS for all alternating fin cases with an unsteady flow ($Re \geq 1800$). This agreement is however reasonable since there exist a strong relationship between pressure drop and heat transfer [63] that makes Eq. (7) useful also for non-smooth pipes with known f [61]. Since the fin design evaluated here features relatively small fins, the fins effectively represent a rough pipe with f significantly larger than that of a smooth pipe in the intermediate region of $1700 < Re < 2300$. The good agreement with the experimental correlation Eq. (7) also further validate our numerical methodology for cases with fins.

3.3.1. Performance evaluation criterion

It is well established that enhancing the heat transfer rate using surface modifications generally increases the friction factor (and total pressure drop). To assess if the promising alternating helical fin design

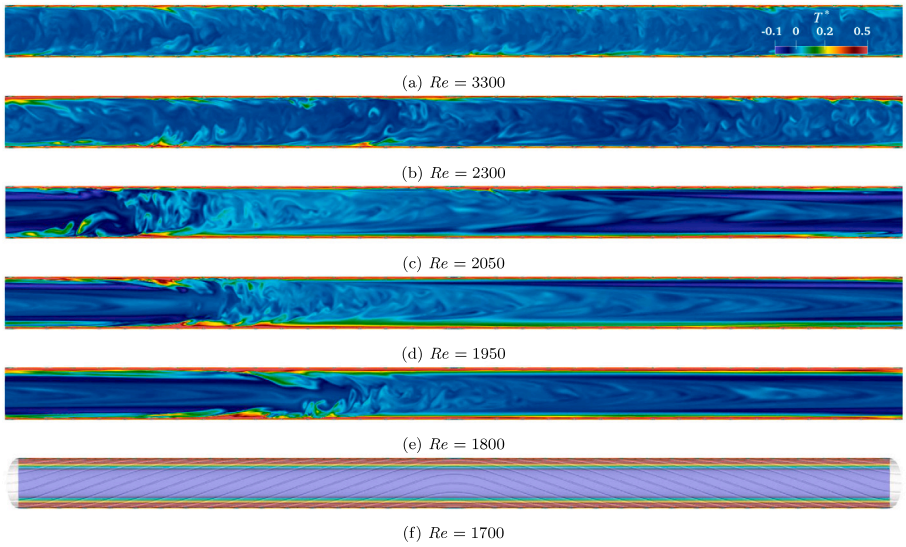

Fig. 8. Instantaneous non-dimensional temperature contours at a cross-section ($z = 0$) of alternating helical fin pipe for $Pr = 75$. The Re decreases from 3300 down to 1700, where the flow becomes laminar. The solutions for $Re < 1700$ are the same as $Re = 1700$ since the flow is laminar. Here, the pipe is compressed to half its actual length ($L/2 = 17.5D$) for visualization purposes and the temperature colour scale in (a) applies to all panels. The inner pipe surface is overlaid in (f) to illustrate the periodic geometry used in all cases (a)–(f). The cases (c)–(e) with $Re < Re_c$ show localized regions of more intense mixing rather than the relatively homogeneous mixing observed in (a)–(b) where $Re \geq Re_c$. The localized mixing regions are not stationary in the reference frame of the pipe but are advected downstream with the bulk flow.

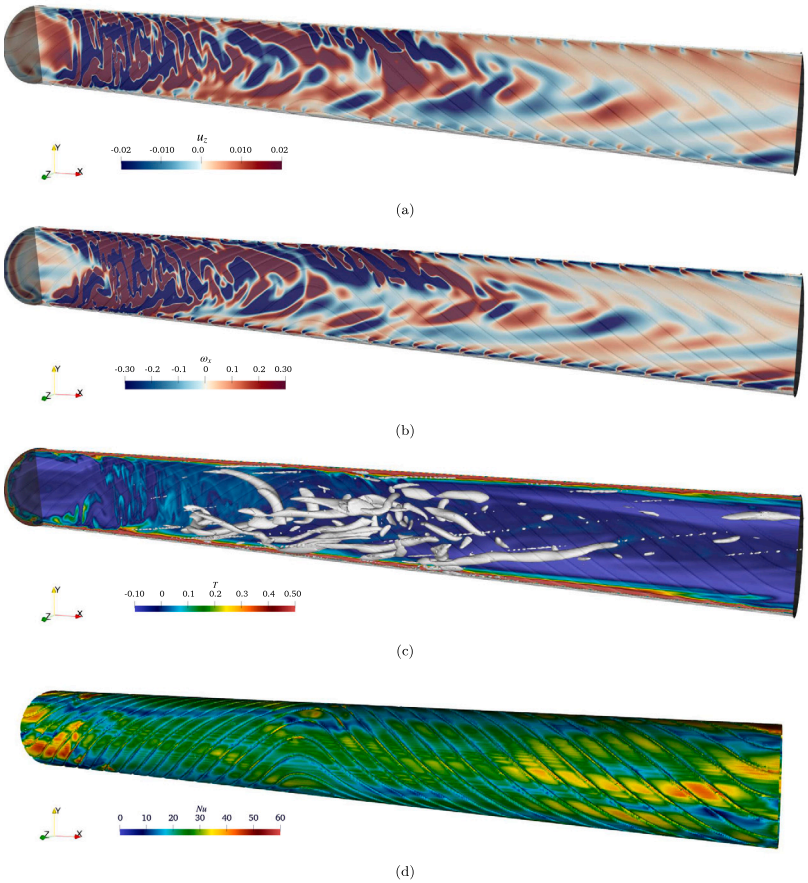

Fig. 9. Instantaneous non-dimensional (a): u_z/U_b velocity (b): $\omega_x D/U_b$ vorticity (c): temperature and Q-criterion iso-surface ($Q = 4$) and (d): local $Nu(\boldsymbol{x}, t)$-contours of the alternating helical fin pipe at $Re = 2050$ (the same instant as in Fig. 8(c)). In (a)–(c), the contours are shown at the cross-sections $z = 0$ and $x = 0$ and L. The pipe length is compressed to $L/4 = 8.75D$ to better show the entire flow field. The inner pipe wall is included as an overlaid transparent surface on (a)–(c).

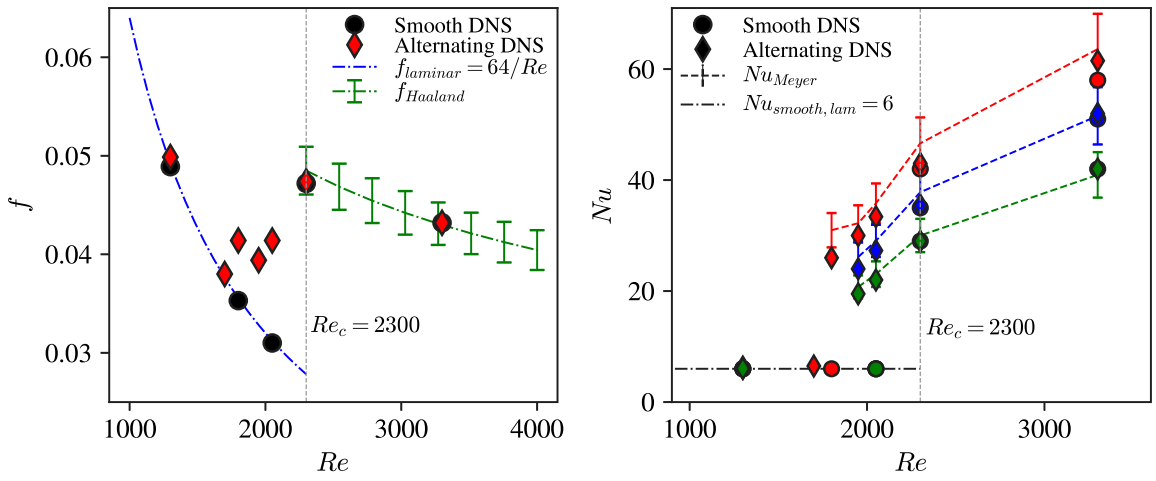

Fig. 10. Time-averaged DNS results from the promising alternating helical fin design ($L = 35D$, $h_{fin}/D = 0.015$, $n_{fin} = 16$ and $\omega_{fin} = 360°$) and a smooth pipe. (a): Predicted friction factor, the laminar solution for smooth pipes and the correlation by Haaland [59] (±5%). An excellent agreement is observed with the laminar solution and the correlation for the smooth pipes but an earlier transition to an unsteady flow (departure from the laminar solution at lower Re) with the alternating fin design. (b): Predicted heat transfer coefficients (Nu) and comparison to the laminar solution for smooth pipes and the correlation of Meyer et al. [61] Eq. (7) evaluated using f from our DNS of the alternating fin design in (a) (±10%). The red, blue and green colours represent cases with $Pr = 75, 40$ and 20, respectively. The earlier transition to an unsteady flow with the alternating fin design causes significantly enhanced heat transfer rates (about 300 – 600% higher than the smooth pipe) in the intermediate range of about $1700 < Re < 2300$. (For interpretation of the references to colour in this figure legend, the reader is referred to the web version of this article.)

Table 6
Nondimensional parameters from the DNS simulations of the promising alternating helical fin design ($L = 35D$, $h_{fin}/D = 0.015$, $n_{fin} = 16$, $\omega_{fin} = 360°$) and the smooth pipe ($L = 8.8D$).

Pipe	Re	Pr	Nu	f	Flow	Pipe	Re	Pr	Nu	f	Flow
Alt. fin	1300	75	6.2	0.0499	laminar	Smooth	1300	75	6	0.0489	laminar
Alt. fin	1300	40	6.1	–	laminar	Smooth	1300	40	6	–	laminar
Alt. fin	1300	20	6.06	–	laminar	Smooth	1300	20	6	–	laminar
Alt. fin	1700	75	6.5	0.038	laminar						
Alt. fin	1800	75	26	0.0414	unsteady	Smooth	1800	75	6	0.0353	laminar
						Smooth	1800	40	6	–	laminar
						Smooth	1800	20	6	–	laminar
Alt. fin	1950	75	30	0.0394	unsteady						
Alt. fin	1950	40	24	–	unsteady						
Alt. fin	1950	20	19.5	–	unsteady						
Alt. fin	2050	75	33.4	0.0414	unsteady	Smooth	2050	75	6	0.031	laminar
Alt. fin	2050	40	27.3	–	unsteady	Smooth	2050	40	6	–	laminar
Alt. fin	2050	20	22	–	unsteady	Smooth	2050	20	6	–	laminar
Alt. fin	2300	75	43	0.0474	unsteady	Smooth	2300	75	42	0.0472	unsteady
Alt. fin	2300	40	35.5	–	unsteady	Smooth	2300	40	35	–	unsteady
Alt. fin	2300	20	29	–	unsteady	Smooth	2300	20	29	–	unsteady
Alt. fin	3300	75	61.5	0.0432	unsteady	Smooth	3300	75	58	0.0432	unsteady
Alt. fin	3300	40	52	–	unsteady	Smooth	3300	40	51	–	unsteady
Alt. fin	3300	20	42	–	unsteady	Smooth	3300	20	42	–	unsteady

performs better than a smooth pipe in terms of energy efficiency, it can be useful to compute a so-called Performance Evaluation Criterion

$$PEC_P = \frac{Nu_{mod}/Nu_{smooth}}{(f_{mod}/f_{smooth})^{(1/3)}}, \tag{8}$$

that evaluates the increased heat transfer for a constant pumping power. Or, alternatively, for the case of a constant flow rate

$$PEC_V = \frac{Nu_{mod}/Nu_{smooth}}{f_{mod}/f_{smooth}}, \tag{9}$$

[14,35,44,64]. Here, f and Nu for the alternating helical fin and smooth pipes are evaluated at the same Re. The obtained PEC-values for our cases are shown in Fig. 11, where a value above 1 indicates an advantageous design. The values for the smooth pipe at $Re = 1700$ and 1950 (where we lack DNS data) are taken as the laminar solution $f = 64/Re$ and $Nu = 6$ since the flow is laminar until at least $Re = 2050$. The top panel shows all PEC-values while the bottom is a zoomed-in view close to $PEC = 1$. Although the friction factor for the modified pipe is somewhat higher between $1700 < Re < 2300$, the significantly enhanced Nu here gives a PEC between 3 and 5 indicating a superior performance at these operating conditions. In the bottom panel, we observe $PEC \gtrapprox 1$ for all other cases. Overall, these values suggest that the alternating helical fin design performs as well or better than the smooth pipe for almost all relevant operating conditions.

It should be noted, however, that many geothermal systems equipped with inverter-controlled circulation pumps are regulated to maintain a constant inlet–outlet temperature difference rather than strictly constant flow rate or constant pumping power. In such systems, enhanced heat transfer from finned pipes may lead simultaneously to reduced flow rate and pumping power. Consequently, no single PEC-definition is universally representative of all geothermal applications.

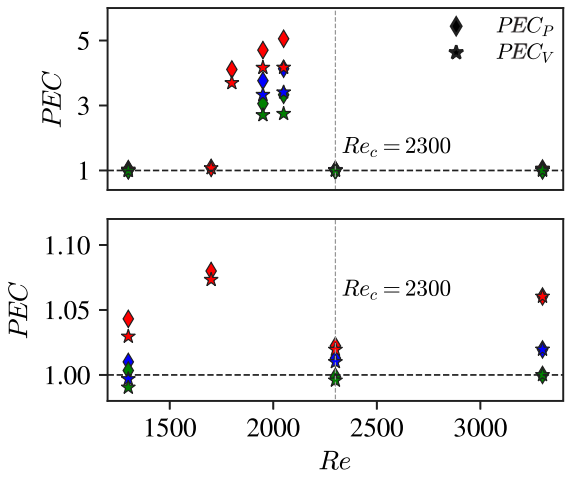

Fig. 11. Performance evaluation criterion for a constant pumping power PEC_P and constant flow rate PEC_V for our promising alternating helical fin design versus Re for all cases in Table 6. The top panel shows all the data while the bottom is a zoomed-in view close to $PEC = 1$ to show the differences for the cases where the flow type is the same for the smooth and alternating helical fin design. The value $Re_c = 2300$ indicates the classical transition to turbulence for a smooth pipe and the red, blue and green colours represent cases with $Pr = 75, 40$ and 20, respectively. (For interpretation of the references to colour in this figure legend, the reader is referred to the web version of this article.)

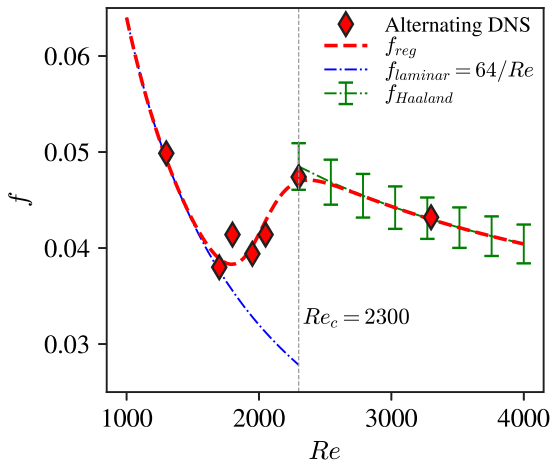

Fig. 12. Regression model f_{reg} of the friction factor predicted for the promising alternating helical fin design. Since f is not significantly higher than that of a smooth pipe outside of the transition region $1700<Re<2300$, the model is constructed as a smooth transition from the laminar to the turbulent formulas for smooth pipes.

However, by including both PEC_P and PEC_V, we provide a basis for comparison across the most relevant operating scenarios.

3.4. Regression models

For convenience, we also provide regression models for f and Nu of the promising alternating helical fin design evaluated in Section 3.3. Since f for this design is practically that of smooth pipes outside of the interval $1700<Re<2300$, f_{reg} can be expressed as an interpolation between the laminar $(64/Re)$ to the turbulent formulas [59] for the smooth pipe as

$$w = \left(1 + \exp\left[-5\left(\frac{Re - 1700}{2300 - 1700} - 0.5\right)\right]\right)^{-1}, \tag{10}$$

$$f_{reg} = (1 - w)\frac{64}{Re} + w\left[-1.8\log_{10}\left(\frac{6.9}{Re}\right)\right]^{-2}. \tag{11}$$

This regression in the relevant interval of Re is shown in Fig. 12 together with the DNS predictions and laminar/turbulent formulas for the smooth pipe.

The heat transfer rate for the promising alternating helical fin design before and after the transition at $Re \approx 1700$ can be well described by the regression

$$Nu^{reg}_{lam} = \sqrt{Nu^2_{smooth,lam} + \left[(5.5 \times 10^{-7})Re^{1.77}Pr^{0.5}\right]^2} \quad \text{for} \quad 0 \le Re \le 1700, \tag{12}$$

$$Nu^{reg}_{turb} = \sqrt{Nu^2_{smooth,lam} + \left[0.86(Re - 1699)^{0.39}Pr^{0.32}\right]^2} \quad \text{for} \quad 1700 < Re \lessapprox 3300, \tag{13}$$

where the absolute standard deviation is 0.005 and 1.42 and the coefficient of determination $R^2 = 0.999$ and $R^2 = 0.988$, respectively for the two expressions. A plot of the regression plane in the (Re, Pr)-phase-space and the data points for the alternating helical fin design are shown in Fig. 13. Here, $Nu_{smooth,lam} = 6$ as previously derived. However, to better approximate the heat transfer at conditions relevant to the geothermal systems (assuming a constant wall temperature without a uniform cooling term), the value $Nu_{smooth,lam} = 3.66$ should be used in Eqs. (12) and (13) instead.

4. Conclusions

We perform Direct Numerical Simulations (DNS) of the hydro- and thermodynamics in smooth pipes and pipes with internal fins to assess the thermohydraulic performance of the fin design at conditions relevant for geothermal heating systems (approximately $1300 \le Re \le 3300$ and $20 \le Pr \le 75$). The simulations show that the alternating helical fin design is the most effective at triggering an unsteady flow at $Re < 2300$ compared to straight fins, continuous helical fins and smooth pipe designs. The alternating helical fin design is therefore chosen for additional parameter studies. With this design, we show that a fin height of about $0.025D$ or less is a suitable choice, giving an acceptable increase of the friction factor at higher flow rates ($Re = 3300$). We also show that about 24 fins or more, with an equal circumferential distribution, is not advantageous for inducing an unsteady flow at $Re < 2300$. Moreover, we assess the influence of the fin twist rate in the alternating helical design on the flow behaviour. Here, we find that the twist rate should be at least 45° during the length of $L/2 = 17.5D$ in the pipe axial direction to induce an unsteady flow down to $Re \approx 1800$.

Based on the parameter analysis, a promising design of alternating helical fins with $L = 35D$, $h_{fin}/D = 0.015$, $n_{fin} = 16$ and $\omega_{fin} = 360°$ is chosen for a detailed evaluation and comparison with the performance of a smooth pipe in the industrially relevant intervals of $1300 \le Re \le 3300$ and $20 \le Pr \le 75$. The simulations show that the promising fin design triggers an unsteady flow and a significantly enhanced heat transfer rate (compared to a smooth pipe) of about $300 - 600\%$ in the intermediate region of $1700<Re<2300$. Outside of this region, the results suggest a few per cent higher friction factor (about 2% higher at $Re = 1300$ but practically the same at $Re \ge 2300$) and heat transfer rate for the alternating helical fin design. We compute a performance evaluation criterion PEC for heat exchanger applications that shows values of up to 5 in the intermediate region and $PEC \gtrapprox 1$ for all other cases. This suggests that the alternating helical fin design has superior performance in the intermediate region $1700<Re<2300$ and slightly better or similar performance as the smooth pipe outside of this region. These characteristics are highly suitable for geothermal collector systems that often operate in the transitional regime and where the friction factor should be kept as low as possible at high flow rates. That the proposed finned collector design enhances heat transfer at low flow rates enables in general a reduction in the required borehole length of the VGHE with relatively low additional manufacturing costs (using plastic extrusion-processes) compared to smooth pipes. Since

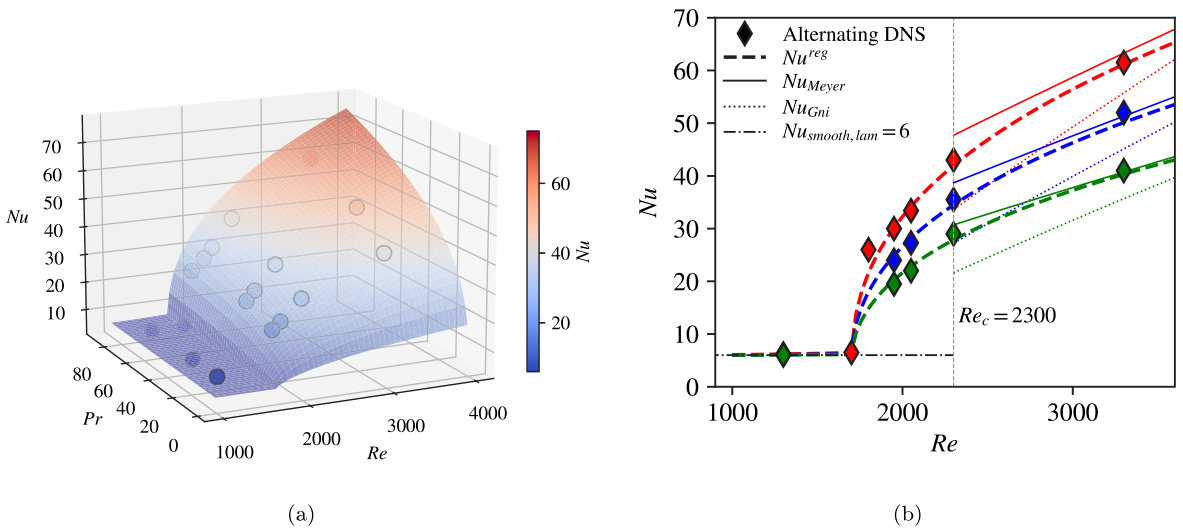

Fig. 13. (a): Regression model Nu^{reg} (Eqs. (12) and (13)) in the (Re, Pr)-phase-space for the alternating helical fin design and the corresponding DNS data points. (b): Regression model Nu^{reg} (Eqs. (12) and (13)) vs. Re of the alternating helical fin design, the corresponding DNS data points and comparison to the solutions for smooth pipes in the laminar and turbulent regime (Eq. (6) and Eq. (7) evaluated using Eq. (5)). The red, blue and green colours represent cases with $Pr = 75, 40$ and 20, respectively. For all Pr here, Nu^{reg} lies in between Nu_{Meyer} and Nu_{Gni} at $Re > 2300$ and approaches Nu_{Meyer} closely at $Re > 3000$. (For interpretation of the references to colour in this figure legend, the reader is referred to the web version of this article.)

drilling may account for 30%–60% of total geothermal system costs, the proposed finned tube demonstrates both practical and economic benefits for industrial installations and supports renewable heating plans such as *RePowerEU*.

Additionally, regression models are provided for the friction factor (Eq. (11)) and the Nusselt number (Eqs. (12) and (13)), for the promising alternating helical fin design valid for laminar and unsteady flow conditions.

The use of DNS in the present study is essential to accurately predict the additional mixing induced by the pipe modifications and to capture the transition to turbulent flow. However, DNS is computationally expensive, which limits the number of designs that can be evaluated, and the promising alternating helical fin configuration identified here is therefore not formally optimized. The cross-sectional shape of the fins is also fixed in the present study, presenting an additional opportunity for performance improvement. While the study does not aim to determine an optimal collector pipe design, the parametric analysis provides valuable insights into the influence of key geometrical and thermohydraulic parameters. Optimization of such systems depends strongly on site-specific conditions, operational requirements, and manufacturing constraints, making a universal optimum difficult to define. Nonetheless, the results highlight promising configurations that outperform conventional smooth pipes and suggest that using computationally cheaper methods in combination with advanced optimization techniques, such as surrogate-based optimization [47,65], could further enhance thermohydraulic performance in future work.

The present work is limited to the convective heat transfer inside the heat exchanger pipe. Conjugate heat transfer analysis that includes the pipe wall, and analysis of how the altered pipe thermal resistance influences the total borehole thermal resistance in geothermal applications, can both further our understanding on how the internally finned tubes perform at system levels.

The internal fin designs considered in this work are evaluated at conditions relevant to geothermal collector pipes. The methodology and results are, however, applicable to any heat exchanger pipe operating at similar conditions. The findings therefore promote further studies into how the alternating helical fin design can be used to trigger unsteady flow and enhance heat transfer at other operating conditions and for other performance considerations.

CRediT authorship contribution statement

Niklas Hidman: Writing – original draft, Visualization, Validation, Methodology, Investigation, Formal analysis, Conceptualization. **Daniel Almgren:** Writing – review & editing, Supervision, Resources, Project administration, Investigation, Conceptualization. **Kim Johansson:** Writing – review & editing, Supervision, Resources, Project administration, Investigation, Conceptualization. **Eskil Nilsson:** Writing – review & editing, Supervision, Resources, Project administration, Methodology, Investigation, Conceptualization.

Declaration of competing interest

The authors declare that they have no known competing financial interests or personal relationships that could have appeared to influence the work reported in this paper.

Acknowledgements

This work was funded by MouviTech Sweden AB.

Data availability

Data will be made available on request.

References

[1] K. Ingrid Stober, Geothermal Energy - From Theoretical Models to Exploration and Development, Springer Cham, Switzerland, 2021.
[2] A. Jahanbin, Thermal performance of the vertical ground heat exchanger with a novel elliptical single U-tube, Geothermics 86 (2020) 101804.
[3] J.S. Figueira, A. García Gil, A. Vieira, A.K. Michopoulos, D.P. Boon, F. Loveridge, F. Cecinato, G. Götzl, J. Epting, K. Zosseder, M. Bloemendal, M. Woods, P. Christodoulides, P.J. Vardon, S.P. Borg, S. Erbs Poulsen, T.R. Andersen, Shallow geothermal energy systems for district heating and cooling networks: Review and technological progression through case studies, Renew. Energy 236 (2024) 121436.
[4] S. Javed, J. Spitler, Accuracy of borehole thermal resistance calculation methods for grouted single U-tube ground heat exchangers, Appl. Energy 187 (2017) 790–806.
[5] J.D. Spitler, S. Javed, R.K. Ramstad, Natural convection in groundwater-filled boreholes used as ground heat exchangers, Appl. Energy 164 (2016) 352–365.

[6] G. Hellström, Ground Heat Storage, Thermal Analysis of Duct Storage Systems, I. Theory (Ph.D. thesis), University of Lund, 1991, pp. 1–262.
[7] H. Javadi, S.S.M. Ajarostaghi, M. Pourfallah, M. Zaboli, Performance analysis of helical ground heat exchangers with different configurations, Appl. Therm. Eng. 154 (2019) 24–36.
[8] M. Roshani, M. Hosseini, A. Ranjbar, A. Torbatinejad, Enhancing geothermal heat pump efficiency with fin creation and microencapsulated PCM: A numerical study, J. Energy Storage 95 (2024) 112664.
[9] M.H. Chaudhry, Applied Hydraulic Transients, vol. 415, Springer, 2014.
[10] S.M. Ghiaasiaan, Two-Phase Flow, Boiling, and Condensation: in Conventional and Miniature Systems, Cambridge University Press, 2017.
[11] R.K. Shah, D.P. Sekulic, Fundamentals of Heat Exchanger Design, John Wiley & Sons, 2003.
[12] R.L. Webb, N.-H. Kim, Principles of Enhanced Heat Transfer, Taylor & Francis, 2005.
[13] M.H. Mousa, N. Miljkovic, K. Nawaz, Review of heat transfer enhancement techniques for single phase flows, Renew. Sustain. Energy Rev. 137 (2021) 110566.
[14] S. Liu, M. Sakr, A comprehensive review on passive heat transfer enhancements in pipe exchangers, Renew. Sustain. Energy Rev. 19 (2013) 64–81.
[15] L. Liebenberg, J.P. Meyer, In-tube passive heat transfer enhancement in the process industry, Appl. Therm. Eng. 27 (16) (2007) 2713–2726.
[16] J. Meyer, S. Abolarin, Heat transfer and pressure drop in the transitional flow regime for a smooth circular tube with twisted tape inserts and a square-edged inlet, Int. J. Heat Mass Transfer 117 (2018) 11–29.
[17] S. Bhattacharyya, A.C. Benim, H. Chattopadhyay, A. Banerjee, Experimental investigation of heat transfer performance of corrugated tube with spring tape inserts, Exp. Heat Transfer 32 (5) (2019) 411–425.
[18] A. Garcia, P.G. Vicente, A. Viedma, Experimental study of heat transfer enhancement with wire coil inserts in laminar-transition-turbulent regimes at different Prandtl numbers, Int. J. Heat Mass Transfer 48 (21–22) (2005) 4640–4651.
[19] B. Yu, J. Nie, Q. Wang, W. Tao, Experimental study on the pressure drop and heat transfer characteristics of tubes with internal wave-like longitudinal fins, Heat Mass Transf. 35 (1) (1999) 65–73.
[20] L.D. Tijing, B.C. Pak, B.J. Baek, D.H. Lee, A study on heat transfer enhancement using straight and twisted internal fin inserts, Int. Commun. Heat Mass Transfer 33 (6) (2006) 719–726.
[21] R. Karwa, B. Maheshwari, N. Karwa, Experimental study of heat transfer enhancement in an asymmetrically heated rectangular duct with perforated baffles, Int. Commun. Heat Mass Transfer 32 (1–2) (2005) 275–284.
[22] J. Chen, P. Zhao, Q. Wang, M. Zeng, Experimental investigation of shell-side performance and optimal design of shell-and-tube heat exchanger with different flower baffles, Heat Transf. Eng. 42 (7) (2021) 613–626.
[23] T. Carnavos, Heat transfer performance of internally finned tubes in turbulent flow, Heat Transf. Eng. 1 (4) (1980) 32–37.
[24] J. Min, R.L. Webb, Numerical analyses of effects of tube shape on performance of a finned tube heat exchanger, J. Enhanc. Heat Transf. 11 (1) (2004).
[25] A. Al-Sarkhi, E. Abu-Nada, Characteristics of forced convection heat transfer in vertical internally finned tube, Int. Commun. Heat Mass Transfer 32 (3–4) (2005) 557–564.
[26] C. Ho, T. Chen, Collector efficiency improvement of recyclic double-pass sheet-and-tube solar water heaters with internal fins attached, Renew. Energy 33 (4) (2008) 655–664.
[27] L. Liu, Z. Cao, T. Shen, L. Zhang, L. Zhang, Experimental and numerical investigation on flow and heat transfer characteristics of a multi-waves internally spiral finned tube, Int. J. Heat Mass Transfer 172 (2021) 121104.
[28] Y.-W. Pai, R.-H. Yeh, Experimental investigation of heat transfer and pressure drop characteristics of internal finned tubes, Int. J. Heat Mass Transfer 183 (2022) 122183.
[29] H.K. Pazarlıoğlu, E. Gürsoy, M. Gürdal, Z. Said, K. Arslan, E. Gedik, Numerical simulation of sudden expansion tubes with ag-mgo nanofluid and innovative fin structure: A thermo-fluidic analysis, Int. J. Heat Fluid Flow 108 (2024) 109448.
[30] Y.-P. Tu, H.-T. Lin, R.-H. Yeh, Experimental study of fully developed turbulent flow in internally finned tubes, J. Enhanc. Heat Transf. 32 (2025).
[31] D.L. Gee, R. Webb, Forced convection heat transfer in helically rib-roughened tubes, Int. J. Heat Mass Transfer 23 (8) (1980) 1127–1136.
[32] T. Ravigururajan, A. Bergles, Development and verification of general correlations for pressure drop and heat transfer in single-phase turbulent flow in enhanced tubes, Exp. Therm. Fluid Sci. 13 (1) (1996) 55–70.
[33] R. Webb, R. Narayanamurthy, P. Thors, Heat transfer and friction characteristics of internal helical-rib roughness, J. Heat Transf. 122 (1) (2000) 134–142.
[34] X.-w. Li, J.-a. Meng, Z.-y. Guo, Turbulent flow and heat transfer in discrete double inclined ribs tube, Int. J. Heat Mass Transfer 52 (3–4) (2009) 962–970.
[35] N. Zheng, W. Liu, Z. Liu, P. Liu, F. Shan, A numerical study on heat transfer enhancement and the flow structure in a heat exchanger tube with discrete double inclined ribs, Appl. Therm. Eng. 90 (2015) 232–241.
[36] N. Hidman, A. Åkesjö, M. Gourdon, A. Jongsma, H. Ström, G. Sardina, S. Sasic, How surface modifications enhance vertical falling film evaporation, J. Fluid Mech. 997 (2024) A17.
[37] S. Pethkool, S. Eiamsa-Ard, S. Kwankaomeng, P. Promvonge, Turbulent heat transfer enhancement in a heat exchanger using helically corrugated tube, Int. Commun. Heat Mass Transfer 38 (3) (2011) 340–347.
[38] J. Hærvig, K. Sørensen, T.J. Condra, On the fully-developed heat transfer enhancing flow field in sinusoidally, spirally corrugated tubes using computational fluid dynamics, Int. J. Heat Mass Transfer 106 (2017) 1051–1062.
[39] J. Córcoles, J. Moya-Rico, A. Molina, J. Almendros-Ibáñez, Numerical and experimental study of the heat transfer process in a double pipe heat exchanger with inner corrugated tubes, Int. J. Therm. Sci. 158 (2020) 106526.
[40] J.-y. Qian, C. Yang, M.-r. Chen, Z.-j. Jin, Thermohydraulic performance evaluation of multi-start spirally corrugated tubes, Int. J. Heat Mass Transfer 156 (2020) 119876.
[41] G.G. Cruz, M.A. Mendes, J.M. Pereira, H. Santos, A. Nikulin, A.S. Moita, Experimental and numerical characterization of single-phase pressure drop and heat transfer enhancement in helical corrugated tubes, Int. J. Heat Mass Transfer 179 (2021) 121632.
[42] W.-T. Ji, A.M. Jacobi, Y.-L. He, W.-Q. Tao, Summary and evaluation on single-phase heat transfer enhancement techniques of liquid laminar and turbulent pipe flow, Int. J. Heat Mass Transfer 88 (2015) 735–754.
[43] C. Montagud, J.M. Corberan, Á. Montero, J.F. Urchueguia, Analysis of the energy performance of a ground source heat pump system after five years of operation, Energy Build. 43 (12) (2011) 3618–3626.
[44] J. Fan, W. Ding, J. Zhang, Y. He, W. Tao, A performance evaluation plot of enhanced heat transfer techniques oriented for energy-saving, Int. J. Heat Mass Transfer 52 (1–2) (2009) 33–44.
[45] M.K. Jensen, A. Vlakancic, Technical note experimental investigation of turbulent heat transfer and fluid flow in internally finned tubes, Int. J. Heat Mass Transfer 42 (7) (1999) 1343–1351.
[46] Z. Wang, H. Shang, J. Zhang, Lattice Boltzmann simulations of heat transfer in fully developed periodic incompressible flows, Phys. Rev. E 95 (6) (2017) 063309.
[47] R. Das, B. Kundu, Direct and inverse approaches for analysis and optimization of fins under sensible and latent heat load, Int. J. Heat Mass Transfer 124 (2018) 331–343.
[48] M. Everts, J. Meyer, Heat transfer of developing and fully developed flow in smooth horizontal tubes in the transitional flow regime, Int. J. Heat Mass Transfer 117 (2018) 1331–1351.
[49] K. Avila, D. Moxey, A. De Lozar, M. Avila, D. Barkley, B. Hof, The onset of turbulence in pipe flow, Science 333 (6039) (2011) 192–196.
[50] J. Abraham, E. Sparrow, J. Tong, Heat transfer in all pipe flow regimes: laminar, transitional/intermittent, and turbulent, Int. J. Heat Mass Transfer 52 (3–4) (2009) 557–563.
[51] G. Wadsley, D. Fletcher, A. Ingram, J. Aubin, W.R. Trujillo, M. Simmons, Complexities of the transitional flow regime downstream of a square-edged orifice in a circular pipe, Chem. Eng. Sci. 310 (2025) 121516.
[52] L. Marocco, A. Franco, Direct numerical simulation and RANS comparison of turbulent convective heat transfer in a staggered ribbed channel with high blockage, J. Heat Transf. 139 (2) (2017) 021701.
[53] Å. Melinder, Thermophysical Properties of Aqueous Solutions Used as Secondary Working Fluids (Ph.D. thesis), KTH, 2007.
[54] W. Wagner, A. Pruß, The IAPWS formulation 1995 for the thermodynamic properties of ordinary water substance for general and scientific use, J. Phys. Chem. Ref. Data 31 (2) (2002) 387–535.
[55] S. Popinet, A quadtree-adaptive multigrid solver for the Serre-Green-Naghdi equations, J. Comput. Phys. 302 (2015) 336–358.
[56] H. Johansen, P. Colella, A cartesian grid embedded boundary method for Poisson's equation on irregular domains, J. Comput. Phys. 147 (1) (1998) 60–85.
[57] S. Pirozzoli, J. Romero, M. Fatica, R. Verzicco, P. Orlandi, DNS of passive scalars in turbulent pipe flow, J. Fluid Mech. 940 (2022) A45.
[58] S.B. Pope, Turbulent Flows, IOP Publishing, 2001.
[59] S.E. Haaland, Simple and explicit formulas for the friction factor in turbulent pipe flow, J. Fluids Eng. 105 (1) (1983) 89–90.
[60] V. Gnielinski, Neue gleichungen für den wärme-und den stoffübergang in turbulent durchströmten rohren und kanälen, Forsch. Im Ingenieurwesen A 41 (1975) 8–16.
[61] J.P. Meyer, M. Everts, N. Coetzee, K. Grote, M. Steyn, Heat transfer coefficients of laminar, transitional, quasi-turbulent and turbulent flow in circular tubes, Int. Commun. Heat Mass Transfer 105 (2019) 84–106.
[62] F.P. Incropera, D.P. DeWitt, T.L. Bergman, A.S. Lavine, Fundamentals of Heat and Mass Transfer, vol. 6, Wiley New York, 2006.
[63] M. Everts, J.P. Meyer, Relationship between pressure drop and heat transfer of developing and fully developed flow in smooth horizontal circular tubes in the laminar, transitional, quasi-turbulent and turbulent flow regimes, Int. J. Heat Mass Transfer 117 (2018) 1231–1250.
[64] M. Yilmaz, O. Comakli, S. Yapici, O.N. Sara, Performance evaluation criteria for heat exchangers based on first law analysis, J. Enhanc. Heat Transf. 12 (2) (2005).
[65] S. Koziel, L. Leifsson, Surrogate-Based Modeling and Optimization, Springer, 2013.